HHS Public Access

Author manuscript

Sci Signal. Author manuscript; available in PMC 2023 September 20.

Published in final edited form as:

Sci Signal. 2022 September 20; 15(752): eabl5848. doi:10.1126/scisignal.abl5848.

Clearance of small intestinal crypts involves goblet cell mucus secretion by intracellular granule rupture and enterocyte ion transport

Brendan Dolan,

Anna Ermund,

Beatriz Martinez-Abad,

Malin E.V. Johansson,

Gunnar C. Hansson*

Department of Medical Biochemistry and Cell Biology, University of Gothenburg, 405 30 Gothenburg, Sweden.

Abstract

Goblet cells of the small intestinal crypts contain large numbers of mucin granules that are rapidly discharged to clean bacteria from the crypt. Because acetylcholine released by neuronal and nonneuronal cells controls many aspects of intestinal epithelial function, we used tissue explants and organoids to investigate the response of the small intestinal crypt to cholinergic stimulation. The activation of muscarinic acetylcholine receptors initiated a coordinated and rapid emptying of crypt goblet cells that flushed the crypt contents into the intestinal lumen. Cholinergic stimulation induced an expansion of the granule contents followed by intracellular rupture of the mucin granules. The mucus expanded intracellularly prior to the rupture of the goblet cell apical membrane and continued to expand after its release into the crypt lumen. The goblet cells recovered from membrane rupture and replenished their stores of mucin granules. Mucus secretion from the goblet cells depended on Ca^{2+} signaling, and the expansion of the mucus in the crypt depended on gap junctions and on ion and water transport by enterocytes adjacent to the goblet cells. This distinctive mode of mucus secretion, which we refer to as “expanding secretion,” efficiently cleans the small intestine crypt through coordinated mucus, ion, and fluid secretion by goblet cells and enterocytes.

Introduction

A secreted mucus layer separates the intestinal epithelium from the luminal milieu and its high bacterial content. The secreted gel-forming mucin MUC2 provides the structural

*Corresponding author. gunnar.hansson@medkem.gu.se.

Author contributions: B.D. and G.C.H designed the study. B.D., A.E. and B.M.A. performed experiments and analyzed data. M.E.V.J. and G.C.H supervised the work. B.D. and H.C.H. wrote the manuscript. All authors have approved the manuscript.

Competing interests: The authors declare that they have no competing interests.

Supplementary Materials
Figs. S1–S6.
Movies S1–S23.

framework upon which the mucus layer is constructed (1). A single layer of epithelial cells is responsible for both the absorptive function of the intestinal tract as well as the production and secretion of the mucus. Specialized goblet cells within the epithelium are responsible for the production of MUC2 that, along with other mucus proteins, accumulates in secretory granules localized to an apical region of cell called the theca (2). Mucins are large polymeric glycoproteins that are densely packed within these secretory granules in a process that depends on low pH and high Ca^{2+} concentrations (3). Upon secretion, they become hydrated and undergo a process of rapid expansion. In contrast to the mucus of the colon, the small intestinal mucus is penetrable to bacteria (4). The intervillus mucus is easily removed (5) and is continuously renewed by the villus-resident goblet cells (6). It has been shown that the secretion of ions, in particular HCO_3^-, plays a key role in the formation of a functional small intestinal mucus layer. The secretion of HCO_3^- from enterocytes is required for proper mucus expansion following its secretion from goblet cells (5) and for mucus release in the small intestine (7). Mice lacking a functional cystic fibrosis transmembrane conductance regulator (CFTR), an ion channel that mediates the export of Cl^- and HCO_3^-, suffer from mucus attachment and hyper concentration, leading to ileal obstruction (7, 8) and bacterial overgrowth (9).

Despite the small intestinal mucus being penetrable to bacteria, microbial colonization of the crypt rarely occurs (4). The production of antimicrobial peptides and proteins by the small intestinal epithelium (10–12), in particular Paneth cells, in combination with high rates of mucus secretion from goblet cells at the crypt opening between the villi (6) maintains the sterility of the crypt. These antimicrobial peptides also contribute to the low overall amount of microbial colonization of the overlying mucus. Not all goblet cells in the gastrointestinal tract behave in a similar fashion. The functional specification of gastrointestinal goblet cells is related to their location in the gastrointestinal tract as well as to their position along the crypt-villus axis. Goblet cells found deeper in the crypts of the small intestine retain much of their mucus in intracellular granules and have a slower rate of mucus secretion than those at the crypt opening, whereas goblet cells found in the villus rapidly secrete the mucus that they synthesize, indicating that there is goblet cell specification along the crypt-villus axis (6). This regional goblet cell specification is further highlighted by single-cell transcriptomic analysis of small intestinal and colonic goblet cells (13).

Goblet cell secretion has been divided into two pathways. Baseline secretion is the continuous exocytosis of mucus components required for the constant renewal of the mucus barrier. The cellular mechanisms underlying this mucus secretion pathway have been studied mainly in airway goblet cells (14). This process involves the fusion of single mucin granules with the plasma membrane followed by the release of their contents and involves components of the regulated secretory pathway (15). Another secretory mechanism, commonly referred to as compound exocytosis, is induced by external stimulus and involves intracellular granule fusion and the rapid release of the majority of content stored in the granules of the goblet cell. Previous studies in the colon have suggested a dramatic response that results in cavitation of the goblet cell (16). However, there might be additional types of controlled secretion in the diverse repertoire of goblet cells.

Here, utilizing small intestinal explant tissue and an organoid model from fluorescent mCherry-MUC2 transgenic mice, we have studied mucus secretion in the small intestinal crypt induced by the secretagogue carbachol, an acetylcholine receptor agonist. We found that ion transport by cells adjacent to the goblet cell drove this secretory event, with cell-to-cell communication through gap junctions coordinating the activities of the goblet and absorptive cells involved in this externally induced response. Furthermore, we highlight the sequence of key events in the process of induced goblet cell exocytosis, a distinct process we refer to as "expanding secretion," and its role in the efficient cleaning of the small intestinal crypt as required for minimizing the risk of bacterial crypt invasion and protection of the stem cell population.

Results

Cholinergic stimulation induces a crypt-specific secretory response in the small intestine

Induced secretion by intestinal goblet cells in response to external stimuli such as acetylcholine has been previously reported (17). Cholinergic signaling is known to play an important role in regulating intestinal function such as peristalsis. Potential sources of acetylcholine in the small intestine include cholinergic neurons and immune cells (18), and their interactions with the intestinal epithelium suggest that acetylcholine-induced secretory events may play a role in mucus release. To investigate the effect of cholinergic stimulation on mucus secretion in the ileum, we harvested tissue from C57Bl/6 mice, gently flushed the luminal contents, and measured mucus accumulation using an ex vivo live tissue explant model as previously described (19). Following removal of the longitudinal muscle, we mounted the explanted tissue in a perfusion chamber and the ileal mucus thickness, from mucus surface to crypt opening, was measured to be approximately 200 μm. After we removed the mucus by gentle aspiration, the tissue was allowed to stabilize, and then stimulated basolaterally with the acetylcholine analog carbachol (Cch). Within 20 minutes, the mucus layer had returned to the original thickness (Fig. 1A). In the absence of external stimulation, spontaneous regeneration of the small intestinal mucus does not occur within this period of time (5, 19). Immunofluorescent staining for Muc2 before and after stimulation revealed reduced amounts of Muc2 in crypt goblet cells and an emptied crypt lumen after cholinergic stimulation (Fig. 1B). Our explant mucus measurement system does not allow specific recording of the response of crypt goblet cells. To overcome this, explanted tissue from transgenic mice expressing mCherry-human MUC2 (RedMUC2^{98trTg}) was examined by multi-photon live cell imaging and tracking of the cholinergic response (Fig. 1C & Movie S1). Approximately 2 to 3 minutes after stimulation with Cch, a loss of fluorescence was observed in the secretory cells localized towards the bottom of the crypt, as well as a decreases in the volume of the goblet cell thecae, both of which are indicative of mucus secretion (Fig. 1C & D). No secretory response was observed in cells localized to the upper crypt.

Intestinal organoids have proven to be a powerful tool to study the biology of the small intestinal crypt (20). The crypt-specific nature of the secretory response to Cch suggested that organoids might be useful for studies of secretory responses in the intestinal crypt. Organoids were generated from the mCherry-MUC2 reporter mice and their response to

cholinergic stimulation was investigated using 3-dimensional live cell confocal microscopy (Fig. 1E). The mucus secretion response was confined to goblet cells located to the crypt region (Fig. 1E & Movie S2). Together these results show that cholinergic stimulation of ileal organoids induces a strong mucus secretory response localized to the lower crypt region, similar to live tissue, indicating that organoids may serve as a useful model to investigate the mechanisms of crypt mucus secretion.

Cholinergic stimulation of the small intestinal crypt induces a coordinated secretory response that flushes the crypt lumen

To study the response to cholinergic stimulation in the crypt, we utilized high-speed four-dimensional live cell imaging of mCherry-MUC2 organoid cultures. Prior to stimulation with Cch, crypt goblet cells and the crypt lumen were filled with mucus (Fig. 2A). Stimulation with Cch rapidly induced mucus secretion from goblet cells present in the organoid crypt (Fig. 2A & Movie S3). Cells at the base of the crypt secreted their contents earlier than those further up along the crypt axis (Fig. 2B). The secretory cells responded in an ordered way starting from the bottom of the crypt and moving upwards (Fig. 2B). The goblet cell mucus secretion caused a rapid increase in crypt lumen volume (Fig. 2C). As the contents of the densely packed goblet cell granules were secreted, the luminal fluorescent mucus intensity was quickly reduced as it underwent expansion (Fig. 2A). This increased volume and signal dilution when mucus enters the crypt lumen is likely driven by ion and fluid secretion in response to the cholinergic stimulation (21). Following the mucus expansion in the crypt, the crypt contents were flushed out of the crypt (Fig 2A & C). Finally, we observed empty goblet cells and crypt lumens (Fig. 2A). To examine whether this ordered secretory response occurs in vivo, we examined tissue from Cch-stimulated mice by confocal microscopy (fig. S1A–C). In mice treated with vehicle, granule-filled Paneth and goblet cells were observed at the crypt base (fig. S1A). Following stimulation, the earliest stages of the secretory response could be identified by dilation of the crypt base by the accumulation of fluid, presumably a result of liquid secreted by crypt cells (fig. S1B). Crypts at the later stages of secretion could be identified through the emptying of goblet cells towards the crypt base (fig. S1B + C).

Chrm3 mediates the secretory response of the small intestine to cholinergic stimulation

Cholinergic receptors can be divided into two broad categories: G protein–coupled muscarinic receptors and the ligand-gated ion channel nicotinic receptors (22, 23). Pre-treatment of organoids with the pan-muscarinic receptor antagonist atropine inhibited the Cch-stimulated crypt response (Fig. 2D). Stimulation with nicotine did not induce any secretory response in the crypt (fig. S2A). Together this indicates that the crypt secretory response is driven by muscarinic receptor signaling.

Analysis of RNA-Seq data of goblet and non-goblet cell populations from the ileum (13) revealed that secretory cells are enriched for the expression of transcripts encoding Chrm1 (M_1) and Chrm3 (M_3) (Fig. 2E), these G_q-coupled muscarinic receptors are known to activate Ca^{2+} signaling pathways involved in secretory responses (24). Single-cell RNA-Seq analysis of small intestinal goblet cells (13) allowed for the identification of lower and upper crypt goblet cell populations as well as Paneth cells (fig. S2B). Low amounts of *Chrm1* and

Chrm3 expression were observed in these clusters of cells (fig. S2C). To further explore the cell-specific localization of *Chrm1* and *Chrm3* expression, we examined murine ileal tissue by RNAscope, which showed expression of both transcripts in $MUC2^+$ cells mainly confined to the base of the crypt (Fig. 2F & G).

To investigate the importance of the M_3 receptor for mucus release in response to cholinergic stimulation, we treated small intestinal explants with the M_3-selective antagonist 4-DAMP (25) before Cch addition. This inhibited induced mucus secretion (Fig. 2H), indicating a key role for the M_3 receptor in mediating the tissue response to stimulation. Repeating the same experiment in ileal explants with analysis by multi-photon live imaging were consistent with the inhibition of crypt goblet cell secretion (Fig. 2I & Movie S4) as compared to non-treated controls (Fig. 1C & Movie S1). The inhibitory effect of 4-DAMP was confirmed in the organoid model of small intestinal crypt secretion, where no goblet cell secretion was observed (Fig. 2J & Movie S5) as compared to non-treated controls (Fig. 2A & Movie S3.

To analyze if the crypt is cleaned by the mucus release after Cch stimulation, Alexa Fluor™ 488 10 kDa dextran was applied to the apical surface of live distal small intestine tissue and allowed to diffuse down to the bottom of the crypt before Cch stimulation with or without prior 4-DAMP treatment (Fig. 2K + L & Movies S6 + S7). The fluorescent dextran was efficiently cleared by Cch stimulation (Fig. 2K) unless the M_3 receptor was blocked (Fig. 2L). Together, these results show that muscarinic signaling through the M_3 receptor plays a key role in the small intestinal response to cholinergic stimulation, the crypt-specific secretory response, and flushing of the crypt.

Carbachol-stimulated mucus secretion is driven by Ca^{2+} and requires cell-to-cell communication

Cch-induced flushing of the crypt required both goblet cell mucus release and the accumulation of fluid (Fig. 2K & L), observed as granule release and crypt volume expansion within 10 minutes after stimulation (Fig. 3A & Movie S8). The Cch effect was mediated through the G_q-coupled muscarinic M_3 receptor, the activation of which triggers the release of Ca^{2+} from intracellular through second messengers such as inositol triphosphate and diacylglycerol. The gene encoding the inositol 1,4,5-triphosphate receptor type 3 (*IP3R*) is expressed in crypt goblet cells (fig S3A). Inhibition of IP_3R, with Xestospongin C (26) prior to Cch stimulation prevented goblet cell emptying as well as changes in crypt volume (Fig. 3B & Movie S9). The absence of transcripts coding for ryanodine receptors and the lack of an effect of ryanodine on Cch-induced mucus release (27) (fig S3A–B) indicated that Ca^{2+} release mediated by IP_3R was the most important pathway in this context. In many cell types, the depletion of intracellular Ca^{2+} stores stimulates store-operated Ca^{2+} entry (SOCE), which is mediated by the activation of store-operated Ca^{2+} channels (SOCCs) in the plasma membrane by the endoplasmic reticulum Ca^{2+} sensor STIM (28, 29). Inhibition of STIM activity in organoids with SKF 96365 (30) resulted in incomplete goblet cell emptying and no increase in crypt volume in response to Cch stimulation (Fig 3C & Movie S10). These observations suggest that Cch stimulation of crypt goblet cells through the M_3 receptor triggers intracellular Ca^{2+} release through the

IP_3R pathway and the influx of extracellular Ca^{2+}, both of which are key steps in driving both mucus release and fluid secretion.

Fluid secretion into intestinal crypts is believed to be mediated by enterocyte ion transport and likely involves crosstalk between Ca^{2+} and cyclic adenosine monophosphate (cAMP) signaling cascades (31). Stimulation with forskolin, a cAMP inducer, resulted in a rapid increase in the overall organoid volume (fig. S3C) and flushing of the crypt but did not trigger mucus secretion (fig. S3D & Movie S11). That crypt secretion involved ion transport was also supported by the complete inhibition of goblet cell granule emptying, crypt swelling, and crypt flushing when organoids were treated with the basolateral Na-K-Cl cotransporter 1 (Nkcc1) inhibitor bumetanide (32) (Fig. 3D & Movie S12). Similar results were obtained using low Cl^- conditions (fig. S3E). Expression of the gene encoding Nkcc1 (*Slc12a2*) was higher in small intestinal goblet cells compared to enterocytes (Fig. 3E) and was particularly high in goblet cells at the base of the crypt (fig. S3F) (33).

At the apical membrane, ion secretion is likely mediated by CFTR. The flow of ions through the epithelium is followed by water into the intestinal lumen. Analysis of published RNA-seq data (12) showed that *Cftr* is expressed in several cell types in the small intestinal epithelium, including goblet cells in the base of the crypt (Fig. 3E & F). To explore the role of CFTR in mucus secretion, we generated small intestinal organoids from RedMUC2^{98trTG}/*Cftr*ΔF508 mice. A minimal increase in crypt volume was observed upon Cch stimulation, but the goblet cell theca volume increased slightly and the MUC2 fluorescence pattern changed inside the cells (Fig. 3G & Movie S13). Given that the transport of HCO_3^- through CFTR plays a key role in intestinal mucus expansion (5, 34), we stimulated organoids kept in HCO_3^- free buffer with Cch. The results obtained under these conditions were similar to those in CFTR-deficient organoids (fig. S3G).

Because anion transport appeared to play a more important role than mucus secretion in crypt flushing, we hypothesized that the movement of ions during Cch-induced crypt flushing depended on crypt enterocytes adjacent to goblet cells rather than on the goblet cells themselves. Separation of these effects is possible through the inhibition of different basolateral K^+ channels. Blocking the activity of the K^+ channel Kcnn4, transcripts for which are enriched in ileal goblet cells at the crypt base (fig. S3H), with clotrimazole (35), did not affect Cch-induced crypt flushing in organoids, but the goblet cells underwent incomplete exocytosis (fig. S3H & Movie S14). *Kcnq1*α and *Kcne3*β transcripts, which encode the subunits of another basolateral voltage-gated K^+ channel, the cAMP-activated channel KcnQ1/KcnE3 (Q1/E3), were also expressed at the base of the crypt in the ileal epithelium (fig. S2I). Inhibition of Q1/E3 in organoids with chromanol 293B (36) before Cch stimulation blocked flushing but did not substantially affect mucus release from goblet cells (fig. S3I & Movie S15). Together, these results suggest that the Cch-induced, Ca^{2+}-dependent release of mucin granules from goblet cells was associated with fluid secretion from enterocytes, not goblet cells, suggesting crosstalk between the two cell types.

Intercellular signaling through gap junctions, likely by Ca^{2+}, could coordinate mucus and ion secretion. To study the importance of gap junction–mediated signaling, we pretreated organoids with carbenoxolone, a gap junction inhibitor (37), prior to Cch stimulation. The

goblet cell granules were emptied, although incompletely, and the mucus remained in the crypt lumen, as indicated by an increase in crypt volume (Fig. 3H & Movie S16). Inhibition of gap junctions together with inhibition of the M_3 receptor (carbenoxolone + 4-DAMP) led to a complete blocking of the Cch-evoked secretory response (Fig. 3I & Movie S17). Together, our results suggest that the small intestinal crypt response to cholinergic signaling is a coordinated response involving mucus-secreting goblet cells and their neighboring enterocytes. The secretory event is initiated in M_3^+ secretory cells in the crypt bottom through the release of Ca^{2+} from intracellular stores followed by signaling to adjacent enterocytes through gap junctions. Ion secretion from the adjacent enterocytes is necessary to complete the mucus expansion to flush out contents of the crypt lumen (Fig. 3J).

Evoked crypt mucus secretion occurs in an ordered manner

Imaging of stimulated mucus secretion in small intestinal explant tissue (Fig. 1C) revealed that secretion starts in secretory cells at the crypt bottom. Electron microscopy confirmed this observation in organoids stimulated with Cch for a short period, after which empty Paneth cells and full goblet cells were observed (Fig. 4A). This suggested that the crypt secretory response starts in the Paneth cells. The mCherry-$MUC2^+$ cells in the crypts of organoids can, as in tissue, be divided into weakly and strongly mCherry-fluorescent cells (Fig. 4B). The weak $mCherry^+$ cells were confined to the very bottom of the crypt, suggesting that these cells were Paneth cells. Their identity was confirmed by examination at higher magnification, which showed that the mCherry-MUC2 was localized to the outer rim of the granules (Fig. 4C), consistent with these structures being the dense-core secretory granules previously described in Paneth cells (38). In contrast, the mCherry-MUC2 signal in secretory cells with strong fluorescence was uniform and dense within the granules, a characteristic of goblet cells (Fig 4D).

Being able to differentiate between Paneth and goblet cells in live imaging experiments allowed us to further explore the secretory response at the base of the crypt and track the secretory responses of the two cell types to cholinergic stimulation. Two minutes following Cch stimulation, a reduction in fluorescence was observed close to the apical pole of the Paneth cell (Fig 4B & Fig. 4E), but no response in the goblet cell was recorded at this time point (Fig. 4B & Fig. 4F). Approximately 90 seconds later the secretory response began in the goblet cell, indicated by a reduction in fluorescence at the apical cell pole as the granule contents were diluted (Fig. 4B & Fig. 4F). At this time, the apical membrane of the Paneth cell appeared to be disrupted as the cell underwent degranulation (Fig. 4B & Fig. 4E). Together these observations suggest that cholinergic signaling triggers secretory cells at the base of the crypt beginning with Paneth cells followed by goblet cell responses.

In Paneth cells, stimulation of muscarinic receptors triggers a sequence of intracellular events leading to degranulation (39). 4-dimensional live imaging of the Paneth cell response to Cch revealed that the secretory event was initiated at the apical pole of the Paneth cell theca (Fig. 4G & Movie S18). Over time, as the response proceeded, secreted material was directly extruded from the cell (Fig. 4G). Fluorescent $MUC2^+$ granules were retained in the basal part of the Paneth cell theca (Fig. 4G). A non-responding goblet cell was also observed near the Paneth cells throughout this time course (Fig. 4G). To further investigate the Paneth

cell response, we examined Cch-stimulated organoids generated from WT mice by electron microscopy. Secretory granules in resting Paneth cells displayed an electron-dense core surrounded by a less dense halo, all contained within a granule membrane (Fig. 4H). Upon stimulation, we observed release of the apical granules followed by cavitation of the Paneth cell with the retention of basal granules (Fig. 4H).

Goblet cell granule release is carefully choreographed

Having noted that Cch-evoked granule release began in the most apical region of the goblet cell theca (Fig. 4B), we performed live 3-D volumetric imaging of the goblet cell theca and granules in mCherry-MUC2 small intestinal organoids with high time resolution. Reconstruction of the dense $MUC2^+$ volume of the goblet cell granules filling up the theca showed how the fluorescence vanished at the cell's apical end (Fig. 5A & Movie S19). The disappearance of granules began at the cell's apical end and appeared as growth of a hollow cleft in the theca (Fig. 5A & Movie 19). Over time, the loss of material at this apical region rapidly grew and spread through the center of the theca (Fig. 5A & Movie S19). Tracking the theca fluorescence over the entire emptying of the goblet cell demonstrated that the initial response involved only the apical theca, with deeper granules initially appearing to be unaffected (Figs. 5B + C & Movie S20). The more peripheral granules were then released over the following minutes. This is also illustrated by the decrease in fluorescence intensities and increased distance of the theca from the apical cell surface over time (Fig. 5C). Near the end of the release of the granule content, only a few granules remained at the bottom of the theca close to the nucleus (Fig. 5D & Movie S21). In summary, the release of goblet cell granules is carefully choreographed, with the release of granules spreading rapidly from the top through the center of the theca to the peripheral granules.

Goblet cell secretion involves intracellular mucin granule rupture before the release of expanded mucus material

Compound exocytosis in mast cells is a variant of conventional vesicle fusion with the cell membrane, with vesicles deep in the cell fusing with more apical vesicles that have already fused with the plasma membrane (40, 41). In compound exocytosis in pancreatic acinar cells, granules fuse together inside the cell prior to fusing with the cell membrane (40, 41). However, the cholinergic-stimulated secretion by the small intestinal crypt goblet cells appears to occur by another mechanism. Higher resolution 4-dimensional imaging of a single goblet cell (Fig. 6A & Movie S22) showed that the individual intensely fluorescent granules disappeared one after the other, starting from the apical cell membrane and spreading to granules deeper in the cell. As the sharp boundary of individual granule contents blurred and disappeared, the fluorescence intensity of the contents decreased relative to intact granules but remained inside the cell (Fig. 6A & B). Imaging analysis did not suggest that the granules were fusing with one another or moving towards the cell membrane; rather they remained at their original location and ruptured in place. The relatively sharp border of an individual granule first became more diffuse before the fluorescent contents mixed with the already accumulated intracellular mucin (Fig. 6A & Movie S22). The fluorescence intensity of the intracellular non-granule mucin was considerably lower than that inside the granule, suggesting not only dilution, but also an altered fluorescence intensity of MUC2. An outer rim of fluorescence corresponding to

the plasma membrane of the cell was observed for more than a minute after stimulation. However, when a considerable portion of the granules had ruptured, the outer cell membrane rim disappeared, suggesting rupture of the cell membrane, and the intracellular fluorescence decreased further as the mucin was released into the lumen of the crypt (Fig. 6A + B & Movie S22).

To study the subcellular changes occurring during the secretory response in more detail, we analyzed small intestinal goblet cells during secretion by electron microscopy. Organoids from WT mice were stimulated with Cch and rapidly fixed and prepared for electron microscopy using tannic acid to improve membrane contrast. Goblet cells from unstimulated organoids contained a densely packed theca filled with mucin granules about 2 μm in diameter (Fig. 6C & fig. S4A). Mucin granules in resting goblet cells displayed a heterogeneous electron density, with some granules containing areas with particularly dense material (Fig. 6C & fig. S4A). All granules were well demarked, often with a visible membrane, suggesting intact granule membranes (Fig. 6C & fig. S4A). Upon Cch stimulation, the goblet cells underwent a series of ultrastructural changes (Fig. 6D–F & fig. S4B–G). In the apical part of the theca, where secretion and the disappearance of mucin granules begin (Fig. 6A), the electron density of the granules decreased (Fig. 6D, fig. S4B), suggesting a change in the organization of the granule contents. Whereas granules in the apical region of the cell displayed this change in electron density, granules deeper in the theca did not show any changes, indicative of an ordered response as suggested from live cell imaging. Detailed examination of the granules in the top of the cell at higher magnification showed that the granule periphery was less distinct and that granule membranes were not always visible but appeared fragmented when observed (Fig. 6D). The expanded granules and the presence of membrane fragments suggest that the granules rupture as their content expands (fig. S4C).

To confirm these observations and to study the earliest stages of the goblet cell response to Cch, we examined individual mucin granules by live cell imaging. As established earlier, the goblet cell response to Cch was mediated through IP_3-triggered release of intracellular Ca^{2+} (Fig. 3B). Staining of tissue sections for the IP_3 receptor, Itpr3, revealed a gradient distribution with the greatest abundance of Itpr3 detected in the base of the crypt (Fig. 6G). High resolution imaging further showed that the Itpr3 signal was interspersed between the secretory granules inside the secretory cells (Fig. 6H), indicative of a smooth endoplasmic reticulum network surrounding the granules. Release of Ca^{2+} from these cellular stores might be what triggers the expansion and bursting of mucin granules in responding goblet cells (Fig. 6I & Movie S23). The volume occupied by granules after Cch stimulation was increased by approximately 80%, indicating a substantial expansion of granule mucus content volume during the earliest stages of the secretory response (Fig. 6J). The observed random pattern of granule expansion is likely caused by the LysoSensor Green dye that accumulates in granules, where it can affect the pH.

Imaging of actively secreting cells suggested that ruptured granule material was retained inside the cell with an intact apical cell membrane (Fig. 6A), and electron microscopy images revealed an intact apical membrane and diffuse intracellular material not contained in granules (Fig. 6E; fig. S4D–F), implying that this cellular mucus material was physically

separated from the mucus in the crypt lumen. The separation of cellular mucus material from luminal content was further supported by live cell imaging of organoids stimulated with acetylcholine, which is rapidly degraded. Under these conditions, goblet cell emptying did not go to completion (fig. S5A), and we observed cellular mucus material separated from luminal contents by an intact apical cell membrane (fig. S5A & S5B). Electron microscopy also indicated that the intracellular material is likely composed of expanded mucus because it had a similar structure as material in the crypt lumen (Fig. 6E). Using organoids from mCherry-MUC2 reporter mice, we performed emission spectrum analysis of luminal mucus and granule mucus in untreated crypts (Fig. 6K). The data showed that extracellular mucus and mucus contained in granules had different emission spectra, indicating that the biophysical conditions within granules and in the crypt lumen altered the emission profile of mCherry. When we measured the mCherry emission spectrum in Cch-treated organoids, we saw a spectrum shift in mucus within granules in the apical region of the theca following treatment that was similar to that observed in luminal mucus, indicating that the conditions inside the granules had been altered (Fig. 6L).

Live imaging suggested that the final stage of the goblet cell response is the rupture of the apical cell membrane and mucus release (Fig. 6A). That goblet cells display a ruptured cell membrane while undergoing mucus release was also suggested by electron microscopy (Fig. 6F, fig. S4G). The intracellular material becomes even less dense after it has left the cell (Fig. 2A), suggesting that additional mucus expansion occurs when it enters the crypt lumen and likely depends on fluid secretion as discussed above.

To establish whether similar secretory events could be observed in vivo, a mouse ileal loop was exposed and stimulated with either vehicle or Cch. In vehicle-treated mice, goblet cells containing intact mucin granules could be observed in the small intestinal crypt (fig. S1D). After stimulation with Cch, changes in goblet cell morphology were observed. Prior to goblet cell emptying, granules at the base of the theca maintained their integrity, whereas those towards the apical pole of the theca were less well-defined (fig. S1F). Cells undergoing secretion showed empty cavities (fig. S1E, S1F & S1G) with accumulated non-granulated mucus remnants at their side. This distribution was expected with formalin fixation because non-crosslinked mucus is lost during tissue processing, and only condensed crosslinked mucus in contact with a preserved tissue remain. Intact granules were seen at the base of the remaining theca (fig. S1G).

We previously reported that sentinel goblet cells (senGC), present only in the colon, are rapidly ejected from the epithelium following secretion (42). To establish the fate of small intestinal crypt goblet cells after secretion, we used live imaging, which showed that they were not ejected from the epithelium up to one hour after secretion (fig. S6A). Because the cells remained in the epithelium, we investigated the ability of these cells to replenish their mucin granule content by imaging the organoids for 24 hours after stimulation with Cch. This showed that cells near the crypt bottom replenished their stores of mucin granules (fig. S6B). Tracking of individual cells showed that after an initial lag, the intensity of mCherry-MUC2 fluorescence increased from 8–10 hours after secretion (fig. S6C). These observations indicate that induced goblet cell secretion in the small intestinal crypt does not result in cell death and is followed by replenishment of the mucin granules.

In summary, small intestinal crypt mucus secretion required a coordinated release of mucus and fluid from goblet and adjacent cells. In small intestinal crypt goblet cells, a series of intracellular events resulted in the secretion of expanded mucus into the crypt lumen (Fig. 6M). The results suggest that the process starts inside apical granules with an intracellular expansion of the granule content and rupture of the granule membrane. Released mucus builds up in the apical cellular compartment, causing a bulging of the intact apical cell membrane, until this eventually leads to a rupture of the cell membrane and rapid release from the cell. After secretion goblet cells most likely undergo a period of cellular repair, followed by replenishment of the mucin granule population while the integrity of the crypt epithelium is maintained. Together the results suggest that goblet cells found in the small intestinal crypt undergo a stimulated secretory response that differs from that previously reported for cells found in the colon and other cells with regulated secretion.

Discussion

Secretagogue-induced intestinal goblet cell secretion was recognized long ago (17), but few studies have since addressed this process. Its physiological importance for intestinal protection has also been underexplored. A major obstacle for progress has been the lack of a cell culture–based model system containing appropriate cell lineages in a physiologically relevant context. The reason for this is easily understood by the current work which clearly shows that more than one specialized cell type is required. The identification of intestinal stem cells (43) and the generation of organoid cultures (44) have enabled the development of robust models for studies of different aspects of crypt biology. Here we utilized small intestinal organoids generated from mCherry-MUC2 reporter mice to study the secretory processes underlying the response to cholinergic stimulation. We found that cholinergic stimulation of small intestinal organoids induced a coordinated secretory response involving the movement of ions across the epithelium along with the rapid induction of mucus secretion. This response was initiated in the crypt bottom, both in culture models and in vivo, was regulated through cell-to-cell communication, and resulted in mucus flushing of the crypt. Finally, we provided insight into the mechanism of secretagogue-induced small intestinal goblet cell exocytosis, a distinct—and possibly unique—secretory mechanism that we prefer to name “expanding secretion”. Our results suggest that the secretory response begins at the apical pole of the cell and then spreads like a wave through the theca of the goblet cell. Mucin granules expand, rupture, and their contents fill the apical part of the cell with expanded mucus that is finally released into the crypt lumen. These events are likely driven by the high expanding tendency of packed granule mucins as they become hydrated.

Cholinergic stimulation of small intestinal tissue is known to induce both ion and mucus secretory responses. Ions, such as HCO_3^-, are key players in the expansion of the mucus following secretion and defects result in mucosal diseases such as cystic fibrosis. Previous studies have shown that the goblet cell response to acetylcholine is in large part confined to the crypt (17), but the interplay between ion movement and mucus secretion in the crypt has not been understood. Localization of the receptors sensitive to cholinergic stimulation to secretory cells at the base of the crypt indicates that the response is initiated by these cells, and inhibition of cell-to-cell communication shows that stimulation of neighboring enterocytes provides the ion movement required to power the response. It has been reported

that mutations that affect human NKCC1 cause defects in goblet cell secretion leading to chronic intestinal inflammation (45). Our results show that disruption of ion movement in the crypt results in an altered goblet cell and mucus transport response, which may represent a stagnation of mucus, making the crypt susceptible to microbial colonization. Here we used pharmacological inhibitors to investigate these cellular processes. The role of off-target effects cannot be discounted; however, the inhibitors we used are the ones commonly used in electrophysiological studies of ion movement, and our observations are in agreement with these studies (5, 46, 47) The synchronization of the response to cholinergic stimulation highlights the importance of studying cellular responses in complex models rather than in isolated cells. Cellular crosstalk and coordination of cellular pathways is likely key to the normal function of the gastrointestinal epithelium. Studies often do not distinguish between responses in the crypt versus the villus and between different cell types even though the cellular composition and cellular function can differ substantially between different regions of the epithelium and between cells within the same region. For example, the small intestinal crypt and villus goblet cells display different gene expression profiles and characteristics, with cells in the villus involved in the rapid turnover of mucus, whereas crypt cells only slowly release their cellular contents in the absence of cholinergic stimulation (6). Our previous studies in the colon have identified specialized goblet cells with functions specific to the colon, the senGCs and the intercrypt goblet cells (icGCs) (13, 42). Our observations highlight the need to use methodology that targets specific tissue locations and the positions of cells within these tissues to obtain physiological understanding of how the tissue behaves as a whole.

The site-specific nature of the cholinergic response, as highlighted by live cell imaging of tissue explants and in vivo stimulation, raises the question as to the possible source of acetylcholine in vivo. The gastrointestinal tract may be home to as many as 100 million nerves and 100,000 extrinsic nerve endings (18). The enteric nervous system is composed of sensory neurons, interneurons, and motor neurons that primarily control peristalsis and the movement of water and electrolytes. Enteric glial cells form a large network throughout the gastrointestinal tract and have been shown to contribute to the regulation of epithelial secretion, and the microbiota has been shown to regulate their homeostasis (48). Although the organoids used in this study lack a neuronal network, similar results were obtained in tissue explants and organoids following Cch stimulation. This suggests that these organoids may serve as a useful system to investigate the role of neurotransmitter molecules on epithelial function. Sensing of the contents of the crypt lumen may trigger localized release of acetylcholine, and non-synaptic signaling through epithelial muscarinic receptors may trigger the crypt-specific secretory response. Mice deficient in *Chrm3* display altered intestinal permeability, increased amounts of proinflammatory cytokines, reduced ability to clear intestinal pathogens (49), and are more susceptible to dextran sulfate sodium (DSS)-induced colitis including the ileum (50). Nonneuronal acetylcholine from immune cells may also be an important factor in regulating the biology of the intestinal crypt (51, 52). Immune cells, such as intraepithelial T cells, may serve as an important source of non-synaptic acetylcholine. These cells are not static and have been shown to move around the subepithelial layers (53). Intraepithelial T cells perform local immune surveillance and have been shown to interact with intestinal epithelial cells specifically at the base of the

crypt (54), and the localized production of T cell–derived acetylcholine has been shown to directly affect the production of Paneth cell antimicrobial peptides (55). The presentation of microbial antigens to intraepithelial T cells by the crypt epithelial cells through the major histocompatibility complex class 2 may trigger the localized release of acetylcholine and the subsequent flushing of microbes from the crypt. Increased numbers of these cells in the small intestine compared to the colon (56) indicates that this crypt-flushing mechanism may be a unique mucosal defense mechanism confined to the small intestine.

The cellular mechanisms underpinning cholinergic-induced goblet cell secretion in the small intestine have been poorly understood. Much of what is known about compound exocytosis has come from studies of pancreatic acinar cells (57), in which the secretory vesicles fuse together prior to fusion with the cell membrane and secretion, hence the name multigranular compound secretion. Studies in the colon have shown that cholinergic-induced secretion is confined to the crypt and that secretion is an ordered process suggested to start at the apical pole of the goblet cell theca (16). These electron microscopy studies suggested that fusion of intracellular granules prior to cell membrane fusion was a key part of the mechanism, as it is in the pancreas. Our results from the small intestine suggest that this is not the case for the small intestinal crypt goblet cells. Exocytosis in these cells possibly follows another mechanism wherein intracellular granule fusion may not be a defining factor. Instead, our observations suggest that the secretory process starts inside the granule where the mucus content changes in its organization by becoming less dense (Fig. 6M). This is concomitant with an increase in the granule volume and rupture of the granule membrane. This occurs while the granules are still inside the cell and the cell membrane remains intact. The accumulation of expanding mucus inside the cell causes the goblet cell to increase in volume and the apical membrane to bulge out. Previous electron microscopy studies of small intestinal tissue by Freeman suggested bulging of the apical cell membrane prior to secretion and expulsion of mucus from goblet cells through a ruptured plasma membrane (58). In fact, an earlier study reported that the cell membrane often appeared to be ruptured when mucus was visualized both within cells and in the lumen (59). Finally, the increased intracellular volume and likely pressure, causes the cell membrane to rupture and the release of the mucus.

The secretory pathway and the sorting to the regulated secretory pathway in the trans-Golgi network is accompanied by a decrease in pH and condensation of the stored material (60). This is reflected in the electron-dense material observed in secretory granules exocrine pancreatic cells as observed by Palade in the 1960s (61). The first event observed here after Cch stimulation was a reduction in the electron density of granules close to the apical cell membrane, suggesting an expansion of the packed mucins. Mucins are packed and condensed within the mucin granules by low pH–triggered N-terminal interactions (62, 63). Upon secretion, the pH quickly increases, allowing the mucins to expand up to 1,000-fold. This requires HCO_3^- as transported by the CFTR channel, defects in which cause cystic fibrosis, which is characterized by altered mucus properties (5, 64). The observed expansion of the granule content in the crypt goblet cell is most likely caused by a pH increase inside of the granules. Because the granule membranes initially appear intact, the event is likely initiated by an opening of one or several ion channels, allowing H^+ to exit or HCO_3^- to enter the granule, or a combination of both. Possible candidates, such as Anion exchange

protein 2 (AE2, also known as SLC4A2), are present in goblet cells and enriched in the small intestinal crypt (13) and in mucin granules (2). Because carbohydrate-rich mucins have the strong tendency to expand due to their high water-binding capacity, the observed rupture of the granule membranes is likely caused by the expansion of granule content. We observed that the mCherry-MUC2 that was released from granules and accumulated inside goblet cells was less fluorescent, had an altered emission spectrum, and displayed reduced electron density than that within the granule, suggesting its further expansion. As the cell volume increases by the accumulation of mucus, the cell membrane is likely ruptured by the increased volume. Once the mucus enters into the crypt lumen, more liquid, ions, and HCO_3^- become available and the mucins can expand further. This results in the flushing of the crypt by the mucus from the goblet cells, which, in combination with the antibacterial factors secreted by from the Paneth cells, efficiently cleans the crypt to maintain its sterility.

In the colon, an evoked goblet cell secretory response is responsible for protecting the crypt from bacterial infiltration and is mediated by specialized senGCs that are not present in the small intestine (42). How the goblet cells in any intestinal region respond to bacterial challenge is not clear. The small intestinal crypt is normally not invaded by microbes due to the high volume of mucus production at the crypt opening and high concentration of Paneth cell–derived antimicrobial peptides (6, 10). However, how this is accomplished and coordinated during acute bacterial invasion is less understood. The observed generation of a mucus plume rich in antimicrobial peptides, which flushes and cleans the crypt, will ensure the expulsion of microorganisms. Although this work was performed in a murine setting and interspecies variation with humans cannot be discounted (65, 66), the protection of the Paneth and stem cells in the bottom of the crypt is of great importance for intestinal epithelium homeostasis. This is especially important in relation to classical ileitis (Crohn's disease) wherein Paneth cell dysfunction has been suggested to be its origin (67, 68).
To flush the contents of the small intestinal crypt, mucus secretion must be accompanied by ion secretion, all in response to external stimuli, acting in unison. This crypt defense mechanism has shed new light on how the small intestinal crypt is protected and how defects or exhaustion could leave the crypt open and susceptible for microbial entrance, a likely early event in the development of Crohn's disease.

Materials and Methods

Mice

Wild type (C57BL/6N; Taconic) mice were obtained from our in-house breeding program, the RedMUC2^{98TR} line was generated previously and expresses mouse Muc2 and recombinant mCherry-human MUC2 (42). To generate RedMUC298^{TR}/*Cftr*ΔF508 mice the RedMUC2^{98TR} line was crossed with *Cftr*ΔF508 mice (69). Mice were housed under standardized conditions of temperature (21–22°C) and illumination (12-hour light/dark cycle) with access to food and water *ad libitum*. Water for RedMUC2^{98TR}/*Cftr*ΔF508 mice was supplemented with polyethylene glycol (17.6 mM), KCl (10 mM), Na_2SO_4 (40 mM), $NaHCO_3$ (84.01 mM) and NaCl (25 mM). Animals were cared for and used in accordance with Swedish animal welfare legislation, which meets the European Convention for the Protection of Vertebrate Animals used for Experimental and other Scientific

Purposes (Council of Europe No. 123, Strasbourg 1985) and the European Union Directive 2010/63/EU on the protection of animals used for scientific purposes. Ethical permissions (2285–19, 3006–20) were obtained from Göteborgs djurförsöksetiska nämnd. Animals were anesthetized with isofluorane followed by cervical dislocation. Animals from 6–15 weeks of age were used.

Mouse ileal organoid lines

Mouse ileal organoids lines were generated from 6-week-old male mice with indicated genotypes as previously described (44). Briefly, the last 3 cm of the small intestine was isolated and luminal content was removed by flushing with PBS. Tissue was then inverted, inflated by filling with 5 mM EDTA in PBS and the ends were tied. Tissue was then incubated in 5 mM EDTA/PBS for 1 hour at 4°C with the EDTA/PBS being replaced every 20 minutes. Isolated crypts were pelleted by centrifugation, resuspended in growth factor reduced Matrigel (Corning) and plated in 24-well plates. Cultures were maintained in Advanced DMEM/F12 (Gibco) supplemented with 1x N2 supplement (Gibco), 1x B27 supplement (Gibco), 1 mM *N*-acetyl-L-cysteine (Sigma Aldrich), 50 ng/ml EGF (Gibco), 500 ng/ml R-spondin 1 (Peprotech) and 100 ng/ml Noggin (Sigma Aldrich) and incubated in a humidified atmosphere containing 5% CO_2 at 37°C. Medium was replaced every second day and organoids were passaged by mechanical fragmentation into crypt domains and seeding in fresh Matrigel. For imaging experiments, organoids were seeded in 10 μl Matrigel drops and maintained for 5 days before experiments.

Mucus measurements

Ex vivo mucus measurements were carried out as described previously (19). Following sacrifice distal ileum was dissected and gently flushed with ice cold oxygenated (95% O_2, 5% CO_2) Kreb's buffer (116 mM NaCl, 1.3 mM $CaCl_2$, 3.6 mM KCL, 1.4 mM K_2HPO_4, 23 mM HCO_3 and 1.2 mM $MgSO_4$). Tissue was kept on ice and opened along the mesenteric border and following removal of the longitudinal muscle layer was mounted in a horizontal perfusion chamber. The mucus layer was visualized by the addition of charcoal and mucus thickness was measured from the mucus surface to the base of the villus. Following initial thickness measurement, mucus was removed by pipetting and tissue was stimulated with 10 μM Cch (Sigma Aldrich) and further measurements were taken every 20 minutes.

Live cell imaging of organoid secretion

Before imaging cell membranes were labeled with CellMask DeepRed (Invitrogen). Following washing in warm PBS, cultures were incubated in staining solution (5 μg/ml in PBS) for 15 minutes at 37°C. Excess stain was removed through washing in PBS and labeled cultures were maintained in culture medium for 1 hour at 37°C before imaging experiments. Prior to stimulation cultures were incubated with inhibitors for 10 minutes at 37°C. Inhibitor concentrations are detailed below. For HCO_3^- free imaging experiments, cultures were incubated in HCO_3^- free imaging buffer (120 mM NaCl, 3.3 mM KH_2PO_4, 0.8 mM K_2HPO_4, 1.2 mM $CaCl_2$, 1.2 mM $MgCl_2$ and 10 mM D-glucose). Experiments under low Cl^- conditions were performed in low Cl^- imaging buffer (5 mM NaCl, 25 mM $NaHCO_3$, 115 mM Na-gluconate, 3.3 mM KH_2PO_4, 0.8 mM K_2HPO_4, 1.2 $CaCl_2$, 1.2 MgCl and 10 mM D-glucose). For experiments measuring mucin granule volume acidic

cell compartments were first labeled with LysoSensor Green DND-189 (5 μM; Invitrogen) for 30 minutes at 37°C. Imaging experiments were performed at 37°C on either a LSM700 inverted confocal system (Carl Zeiss) or a LSM880 inverted confocal system equipped with an Airyscan fast detector (Carl Zeiss). Z-stacks were acquired using either 20x (Plan-Apochromat 20x/0.8 M27) or 40x (LD LCI Plan-Apochromat 40x/1.2 Imm Corr DIC M27) lenses. Long term imaging experiments were performed at 37°C and 5% CO_2 on a Celldiscoverer 7 system (Carl Zeiss), z-stacks were collected using a Plan-Apochromat 20x/0.7 lens (Carl Zeiss).

Ex vivo tissue imaging

Tissue was collected as described for mucus measurements. Following collection tissue was opened along the mesenteric border and the longitudinal muscle was removed. For dextran flushing experiments tissue was mounted in a horizontal perfusion chamber and incubated with dextran (Alexa Fluor 488, 10,000 MW; Invitrogen) added apically for 10 minutes. Following stimulation with Cch tissue z-stacks were collected on an upright LSM700 confocal microscope (Carl Zeiss) using a water Pan-Apochromat 20x/1.0 DIC 75 mm lens (Carl Zeiss). Imaging was performed at 37°C.

For multi-photon imaging tissue was pinned in a 50 mm dish and submerged in Kreb's mannitol buffer (Kreb's buffer containing 10 mM D-mannitol) and imaged with an upright LSM 710 NLO system (Carl Zeiss) equipped with a GaAsP Non-descanned detector and a tunable InSight DeepSee laser (680–1300 nm; Spectra-Physics) using a water Pan-Apochromat 20x/1.0 DIC 75 mm lens (Carl Zeiss). Imaging was performed at 37°C.

In vivo Cch treatment

Mice were anaesthetized with Ketamine/Xylazine and a small vertical incision was made in the abdominal wall to expose the peritoneal cavity. The ileal loop was exposed and bathed in Kreb's mannitol buffer +/− 10 μM Cch at 37°C for up to 10 minutes. Following incubation, the mouse was sacrificed by cervical dislocation, the ileum was removed, flushed with 4% PFA and then fixed with 4% PFA. Following fixation, the tissue was embedded in OCT and processed for microscopy. Secretory cells were identified by staining with Wheat Germ Agglutin (10 μg/ml; Thermo Fisher). Confocal and super resolution images were acquired on a LSM900 upright confocal microscope equipped with an Airyscan2 detector (Carl Zeiss) using a Pan-Apochromat 63x/1.4 Oil DIC M27 lens.

Multi-spectral imaging

Organoids were prepared and cell membranes were labeled as described previously. Multi-spectral imaging experiments were performed at 37°C on an inverted LSM880 confocal microscope and data was collected using the lambda acquisition mode. Multiple spectra were acquired simultaneously from approximately 570 nm to 700 nm in 8.9 nm increments. Emission spectra data was exported using Zen Blue software (Carl Zeiss) and normalized to emission values obtained at 610 nm, the emission maximum of mCherry (70).

Stimulants and inhibitors

Stimulant stock solutions were prepared according to manufacturer's instructions. For mucus measurement and tissue imaging experiments 10 μM Cch (Sigma Aldrich) was provided basolaterally. Stimulants were added to tissue culture medium for organoid imaging experiment at the following concentrations: acetylcholine (20 μM; Sigma Aldrich), Cch (20 μM; Sigma Aldrich), forskolin (100 nM; Cayman Chemical) and nicotine (10 μM; Sigma Aldrich).

Inhibitor stock solutions were prepared according to manufacturer's instructions. For mucus measurement and tissue imaging experiments 4-DAMP (100 nM; Cayman Chemical) was supplied basolaterally. For organoid imaging experiments inhibitors were added to tissue culture medium and incubated with cells for 10 minutes prior to stimulation with Cch. Inhibitors were used at the following concentrations; atropine (50 μM; Sigma Aldrich), physostigmine salicylate (10 μM; Sigma Aldrich), tetraisopropyl pyrophosphoramide (10 μM; Sigma Aldrich), 4-DAMP (100 nM), (−)-Xestospongin C (10 μM; Tocris), SKF 96365 (10 μM; Tocris), carbenoxolone (50 μM; Sigma Aldrich), bumetanide (50μM; Sigma Aldrich), clotrimazole (30 μM; Sigma Aldrich), Chromanol 293B (10 μM; Sigma Aldrich) and Ryanodine (100 nM; Tocris).

RNAscope in situ hybridization

Ileal tissue from wildtype mice was fixed for 16 hours in 4% PFA at 4°C and then embedded in paraffin. Sections were then probed with the following RNAscope probes against *Chrm1* (Probe-Mm-Chrm1-O1-C2; ACD), *Chrm3* (Probe-Mm-Chrm3; ACD) and *Muc2* (Probe-Mm-Muc2 or Probe-Mm-Muc2-C2; ACD) according to manufacturer's instructions using RNAscope multiplex fluorescent detection kit v2 (ACDBio). Following hybridization sections were immunostained with a rabbit anti-EpCAM polyclonal antibody (1:100; Abcam; RRID: AB_1603782) for 1 hr. at room temperature and fluorophore conjugated secondary antibody (1:1000; Thermo Fisher; RRID: AB_2535812).

Analysis of RNA-sequencing and single cell RNA-sequencing datasets

The raw data from the bulk RNA-seq (GSE144363) and scRNA-seq (GSE144364) are deposited in GEO, in the super series GSE144436 (13).

Quality of the bulk RNA-seq data was evaluated using FastQC (version 0.11.2; Babraham Bioinformatics) and the FASTQ files were filtered using Prinseq (version 0.20.3) (71). The alignment was made against the mouse reference genome mm10 using STAR (version 2.5.2b) (72), and the number of mapped reads was calculated with HTseq (version 0.6.1p1) (73) using the stranded reverse protocol. Data normalization, differential expression and statistical analysis were carried out using DESeq2 (version 1.14) in R (74).

The scRNA-seq data were processed with Seurat v3.0 software (75, 76) in R using as random seed 9990. Exclusively cells expressing at least 200 genes and genes present in at minimun 3 cells were considered for further analysis. Cells with a high percentage of mitochondrial genes (> 20%), and with a number of detected genes lower than 800 or higher than 6500 were excluded. Cells expressing *Ptprc* (>1) and cells with low expression of *Muc2*

(<3) were also removed to avoid contamination from immune cells or enterocytes. In total we identified 14794 genes across 3709 cells. The raw data were Log normalized and scaled. To cluster the cells the resolution was set to 0.15 and the dimensions to 1:9. Clustered cells were plotted by a *t*-SNE plot. Differentially expressed genes were statistically analyzed by Wilcoxon Rank Sum test and adjusted p-values were calculated based on Bonferroni correction. The heatmap, the violin and tSNE plots were made in Seurat.

Tissue fixation and immunostaining

Harvested ileal tissue was fixed in either Carnoy's solution (60% dry methanol, 30% chloroform, 10% glacial acetic acid) or 10% neutral buffered formalin. Following fixation tissue was processed for histology and embedded in paraffin wax. Sections were deparaffinized in xylene substitute, rehydrated and underwent heat induced antigen retrieval in 10 mM citrate buffer (pH 6.0). For Muc2 staining sections were blocked in 5% fetal bovine serum for 1 hr. at room temperature prior to incubation with primary antibodies. For Itpr3 staining sections were first permeabilized with 0.02% (w/v) saponin (Sigma Aldrich) in PBS for 10 minutes followed by blocking in 1% BSA (Sigma Aldrich)/10% normal goat serum (DAKO) in PBS for 1 hr. at room temperature. Primary antibodies were added in appropriate blocking buffer and incubated overnight at 4°C. Primary antibodies used were rabbit anti-MUC2 polyclonal antibody (1:2000; Genetex; RRID: AB_1950958) and rabbit anti-Itpr3 polyclonal antibody (1:1000; Millipore; RRID: AB_571029). Following incubation sections were washed with PBS and incubated for 1 hr. at room temperature with Alexa Fluor conjugated secondary antibodies diluted in PBS (1:1000; Thermo Fisher; RRID: AB_143165 and RRID: AB_2535850). Cell nuclei were counterstained with Hoechst 34580 diluted in PBS (5 μg/ml; Sigma Aldrich) for 5 minutes at room temperature. Secretory cells were counterstained with Alexa Fluor 647 conjugated Wheat Germ Agglutinin (WGA) diluted in PBS (10 μg/ml; Invitrogen) for 30 minutes at room temperature. After all staining and washing steps were complete coverslips were mounted using ProLong Gold antifade mountant (Thermo Fisher). Confocal and super resolution images were acquired on a LSM900 upright confocal microscope equipped with an Airyscan2 detector (Carl Zeiss) using a Pan-Apochromat 63x/1.4 Oil DIC M27 lens.

Electron microscopy

Wildtype organoids were stimulated with 20 μM Cch and samples were collected for electron microscopy every 30 seconds post stimulation. In order to capture secretory events samples were rapidly fixed at 37°C using pre-warmed fixing solution (4% glutaraldehyde, 4% formaldehyde, 0.02% sodium azide in 0.5 M Na-cacodylate buffer) for 10 minutes followed by incubation at room temperature for 1–2 hrs. Following washing in cacodylate buffer, samples were post-fixed in 1% osmium tetroxide in 0.1 M Na-cacodylate buffer for 1 h at 4°C. After fixation samples were incubated for 1 h with 1% tannic acid at room temperature, dehydrated and embedded in Hard Plus Resin 812 (Cat# 14115, Electron Microscopy Sciences, Hatfield, PA). Ultra-thin sections (80 nm) were cut on an ultramicrotome (Leica Microsystems, Wetzlar, Germany) using a diamond knife (Diatome, Nidau, Switzerland) and mounted on copper grid supports. Transmission electron microscopic images were acquired with a Talos L120C TEM with a LaB_6 gun and a Ceta CMOS 4k × 4k camera (Thermo Fisher Scientific, Waltham, MA) operated at 120 kV.

Ultra-thin (40 nm) ribbons were sectioned on an ultramicrotome for array tomography (Leica Microsystems, Wetzlar, Germany) using a diamond knife. Sections were mounted on silicon wafers, contrasted with uranyl acetate and lead citrate and imaged with a Gemini II 450 (Carl Zeiss, Oberkochen, Germany) at 2 kV, working distance 4 mm and scan speed 10 using the BSD1 detector.

Image analysis

To quantify overall organoid volume, goblet cell theca volume and crypt volume, confocal z-stack time-series were produced using Zen software (Carl Zeiss) and exported to Imaris (v 9.5; Bitplane). For volume measurements organoid and crypt surfaces were mapped to isosurfaces using the CellMask DeepRed signal and isosurface volumes were tracked over time. Goblet cell theca measurements were performed using a similar strategy except that goblet cell theca volumes were mapped to isosurfaces using the mCherry-MUC2 signal and then tracked with respect to time. Line profiles were generated using the Intensity Profile pluggin in Icy (v 2.1.2.0; BioImage Analysis Lab – Institut Pasteur) following highlighting of regions of interest. Internal areas of organoid crypts were measured using ImageJ (v 1.53c; NIH). All extracted data was exported to Microsoft Excel for normalisation and graphs were drawn using Prism software (v 9.4.0; GraphPad).

Mucin granule volume data was extracted using Zen software. Briefly granule diameter (d) pre and post Cch treatment was measured and granule volume was calculated using the formula; volume = $(4/3)\pi(d/2)^3$.

Analysis of mCherry emission spectra was performed using Zen software (Zen Blue v 3.1; Carl Zeiss). Briefly collected spectral data from regions of interest was unmixed, exported to Excel and normalized to mCherry emission intensity at 610 nm. Graphing of emission spectra and statistical analysis was performed using Prism software.

For long term imaging of organoids, brightfield and fluorescent widefield images were post processed using Fiji (v 1.53f51) by the Difference of Gaussians method. Following post processing 3D projections were generated using the 3D Project pluggin and mCherry signal intensity was tracked over time using the TrackMate pluggin (77).

Statistical analysis

Data analysis was performed using Prism software (v 9.4.0; Graphpad). Group differences were analyzed with Mann-Whitney test or Welch’s test. Paired samples were analyzed with paired t-test. All tests were two-tailed. P-values are shown in figure legends.

Supplementary Material

Refer to Web version on PubMed Central for supplementary material.

Acknowledgements:

The authors acknowledge Dr. Staffan Nilsson (University of Gothenburg) for analysis of the statistics. The authors acknowledge the work of Dr. Elisabeth Nyström (University of Gothenburg) in generating RNA-sequencing

datasets. We also acknowledge the Centre for Cellular Imaging at the University of Gothenburg, Julia Fernandez-Rodriguez, and their support for a National Microscopy Infrastructure (VR-RFI 2016-00968).

Funding:

This work was supported by the European Research Council ERC (694181), National Institute of Allergy and Infectious Diseases (U01AI095473, the content is solely the responsibility of the authors and does not necessarily represent the official views of the NIH), The Knut and Alice Wallenberg Foundation (2017.0028), Swedish Research Council (2017-00958), The Swedish Cancer Foundation (CAN 2017/360), IngaBritt and Arne Lundberg Foundation (2018-0117), Sahlgren's University Hospital (ALFGBG-440741, The ALF agreement 236501), Bill and Melinda Gates Foundation (OPP1202459), and Wilhelm and Martina Lundgren's Foundation.

Data and materials availability:

All data needed to evaluate the conclusions in the paper are present in the paper or the Supplementary Materials. Further information and requests for resources and reagents should be directed to and will be fulfilled by the lead contact, Gunnar C. Hansson (gunnar.hansson@medkem.gu.se).

References and Notes

1. Johansson ME, Hansson GC, Immunological aspects of intestinal mucus and mucins. Nature reviews. Immunology 16, 639–649 (2016).
2. Rodriguez-Pineiro AM et al. , Proteomic study of the mucin granulae in an intestinal goblet cell model. Journal of proteome research 11, 1879–1890 (2012). [PubMed: 22248381]
3. Ambort D et al. , Calcium and pH-dependent packing and release of the gel-forming MUC2 mucin. Proceedings of the National Academy of Sciences of the United States of America 109, 5645–5650 (2012). [PubMed: 22451922]
4. Ermund A, Schutte A, Johansson ME, Gustafsson JK, Hansson GC, Studies of mucus in mouse stomach, small intestine, and colon. I. Gastrointestinal mucus layers have different properties depending on location as well as over the Peyer's patches. American journal of physiology. Gastrointestinal and liver physiology 305, G341–347 (2013). [PubMed: 23832518]
5. Gustafsson JK et al. , Bicarbonate and functional CFTR channel are required for proper mucin secretion and link cystic fibrosis with its mucus phenotype. The Journal of experimental medicine 209, 1263–1272 (2012). [PubMed: 22711878]
6. Schneider H, Pelaseyed T, Svensson F, Johansson MEV, Study of mucin turnover in the small intestine by in vivo labeling. Scientific reports 8, 5760 (2018). [PubMed: 29636525]
7. Schutte A et al. , Microbial-induced meprin beta cleavage in MUC2 mucin and a functional CFTR channel are required to release anchored small intestinal mucus. Proceedings of the National Academy of Sciences of the United States of America 111, 12396–12401 (2014). [PubMed: 25114233]
8. Grubb BR, Boucher RC, Pathophysiology of gene-targeted mouse models for cystic fibrosis. Physiol Rev 79, S193–214 (1999). [PubMed: 9922382]
9. Norkina O, Burnett TG, De Lisle RC, Bacterial overgrowth in the cystic fibrosis transmembrane conductance regulator null mouse small intestine. Infection and immunity 72, 6040–6049 (2004). [PubMed: 15385508]
10. Bevins CL, Salzman NH, Paneth cells, antimicrobial peptides and maintenance of intestinal homeostasis. Nat Rev Microbiol 9, 356–368 (2011). [PubMed: 21423246]
11. Gallo RL, Hooper LV, Epithelial antimicrobial defence of the skin and intestine. Nature reviews. Immunology 12, 503–516 (2012).
12. Meyer-Hoffert U et al. , Secreted enteric antimicrobial activity localises to the mucus surface layer. Gut 57, 764–771 (2008). [PubMed: 18250125]
13. Nystrom EEL et al. , An intercrypt subpopulation of goblet cells is essential for colonic mucus barrier function. Science 372, (2021).

14. Zhu Y et al. , Munc13–2−/− baseline secretion defect reveals source of oligomeric mucins in mouse airways. J Physiol 586, 1977–1992 (2008). [PubMed: 18258655]
15. Jaramillo AM, Azzegagh Z, Tuvim MJ, Dickey BF, Airway Mucin Secretion. Ann Am Thorac Soc 15, S164–S170 (2018). [PubMed: 30431339]
16. Specian RD, Neutra MR, Mechanism of rapid mucus secretion in goblet cells stimulated by acetylcholine. J Cell Biol 85, 626–640 (1980). [PubMed: 7391135]
17. Neutra MR, O'Malley LJ, Specian RD, Regulation of intestinal goblet cell secretion. II. A survey of potential secretagogues. The American journal of physiology 242, G380–387 (1982). [PubMed: 7065260]
18. Yoo BB, Mazmanian SK, The Enteric Network: Interactions between the Immune and Nervous Systems of the Gut. Immunity 46, 910–926 (2017). [PubMed: 28636959]
19. Gustafsson JK et al. , An ex vivo method for studying mucus formation, properties, and thickness in human colonic biopsies and mouse small and large intestinal explants. American journal of physiology. Gastrointestinal and liver physiology 302, G430–438 (2012). [PubMed: 22159279]
20. Clevers H, Modeling Development and Disease with Organoids. Cell 165, 1586–1597 (2016). [PubMed: 27315476]
21. Vega G et al. , Normal Calcium-Activated Anion Secretion in a Mouse Selectively Lacking TMEM16A in Intestinal Epithelium. Front Physiol 10, 694 (2019). [PubMed: 31263421]
22. Changeux JP, The nicotinic acetylcholine receptor: the founding father of the pentameric ligand-gated ion channel superfamily. The Journal of biological chemistry 287, 40207–40215 (2012). [PubMed: 23038257]
23. Wess J, Eglen RM, Gautam D, Muscarinic acetylcholine receptors: mutant mice provide new insights for drug development. Nat Rev Drug Discov 6, 721–733 (2007). [PubMed: 17762886]
24. Caulfield MP, Muscarinic receptors--characterization, coupling and function. Pharmacol Ther 58, 319–379 (1993). [PubMed: 7504306]
25. Doods HN et al. , Selectivity of muscarinic antagonists in radioligand and in vivo experiments for the putative M1, M2 and M3 receptors. J Pharmacol Exp Ther 242, 257–262 (1987). [PubMed: 3612532]
26. Gafni J et al. , Xestospongins: potent membrane permeable blockers of the inositol 1,4,5-trisphosphate receptor. Neuron 19, 723–733 (1997). [PubMed: 9331361]
27. Sutko JL, Airey JA, Welch W, Ruest L, The pharmacology of ryanodine and related compounds. Pharmacol Rev 49, 53–98 (1997). [PubMed: 9085309]
28. Putney JW et al. , The functions of store-operated calcium channels. Biochim Biophys Acta Mol Cell Res 1864, 900–906 (2017). [PubMed: 27913208]
29. Zhou Y et al. , The STIM-Orai coupling interface and gating of the Orai1 channel. Cell Calcium 63, 8–13 (2017). [PubMed: 28087079]
30. Varnai P, Hunyady L, Balla T, STIM and Orai: the long-awaited constituents of store-operated calcium entry. Trends Pharmacol Sci 30, 118–128 (2009). [PubMed: 19187978]
31. Venkatasubramanian J, Ao M, Rao MC, Ion transport in the small intestine. Curr Opin Gastroenterol 26, 123–128 (2010). [PubMed: 20010100]
32. Payne JA, Rivera C, Voipio J, Kaila K, Cation-chloride co-transporters in neuronal communication, development and trauma. Trends Neurosci 26, 199–206 (2003). [PubMed: 12689771]
33. Jakab RL, Collaco AM, Ameen NA, Physiological relevance of cell-specific distribution patterns of CFTR, NKCC1, NBCe1, and NHE3 along the crypt-villus axis in the intestine. American journal of physiology. Gastrointestinal and liver physiology 300, G82–98 (2011). [PubMed: 21030607]
34. Garcia MA, Yang N, Quinton PM, Normal mouse intestinal mucus release requires cystic fibrosis transmembrane regulator-dependent bicarbonate secretion. The Journal of clinical investigation 119, 2613–2622 (2009). [PubMed: 19726884]
35. Wu SN, Li HF, Jan CR, Shen AY, Inhibition of Ca2+-activated K+ current by clotrimazole in rat anterior pituitary GH3 cells. Neuropharmacology 38, 979–989 (1999). [PubMed: 10428416]
36. Schroeder BC et al. , A constitutively open potassium channel formed by KCNQ1 and KCNE3. Nature 403, 196–199 (2000). [PubMed: 10646604]

37. Sagar GD, Larson DM, Carbenoxolone inhibits junctional transfer and upregulates Connexin43 expression by a protein kinase A-dependent pathway. J Cell Biochem 98, 1543–1551 (2006). [PubMed: 16552723]
38. Stahl M et al. , The Muc2 mucin coats murine Paneth cell granules and facilitates their content release and dispersion. American journal of physiology. Gastrointestinal and liver physiology 315, G195–G205 (2018). [PubMed: 29698056]
39. Satoh Y, Ishikawa K, Oomori Y, Takeda S, Ono K, Bethanechol and a G-protein activator, NaF/AlCl3, induce secretory response in Paneth cells of mouse intestine. Cell Tissue Res 269, 213–220 (1992). [PubMed: 1358451]
40. Sanchez E et al. , Syntaxin 3, but not syntaxin 4, is required for mast cell-regulated exocytosis, where it plays a primary role mediating compound exocytosis. The Journal of biological chemistry 294, 3012–3023 (2019). [PubMed: 30563839]
41. Wu LG, Hamid E, Shin W, Chiang HC, Exocytosis and endocytosis: modes, functions, and coupling mechanisms. Annual review of physiology 76, 301–331 (2014).
42. Birchenough GM, Nystrom EE, Johansson ME, Hansson GC, A sentinel goblet cell guards the colonic crypt by triggering Nlrp6-dependent Muc2 secretion. Science 352, 1535–1542 (2016). [PubMed: 27339979]
43. Barker N et al. , Identification of stem cells in small intestine and colon by marker gene Lgr5. Nature 449, 1003–1007 (2007). [PubMed: 17934449]
44. Sato T et al. , Single Lgr5 stem cells build crypt-villus structures in vitro without a mesenchymal niche. Nature 459, 262–265 (2009). [PubMed: 19329995]
45. Koumangoye R, Omer S, Kabeer MH, Delpire E, Novel Human NKCC1 Mutations Cause Defects in Goblet Cell Mucus Secretion and Chronic Inflammation. Cellular and molecular gastroenterology and hepatology 9, 239–255 (2020). [PubMed: 31655271]
46. Gustafsson JK et al. , Carbachol-induced colonic mucus formation requires transport via NKCC1, K(+) channels and CFTR. Pflugers Arch 467, 1403–1415 (2015). [PubMed: 25139191]
47. Flores CA, Melvin JE, Figueroa CD, Sepulveda FV, Abolition of Ca2+-mediated intestinal anion secretion and increased stool dehydration in mice lacking the intermediate conductance Ca2+-dependent K+ channel Kcnn4. J Physiol 583, 705–717 (2007). [PubMed: 17584847]
48. Kabouridis PS et al. , Microbiota controls the homeostasis of glial cells in the gut lamina propria. Neuron 85, 289–295 (2015). [PubMed: 25578362]
49. McLean LP et al. , Type 3 Muscarinic Receptors Contribute to Clearance of Citrobacter rodentium. Inflamm Bowel Dis 21, 1860–1871 (2015). [PubMed: 25985244]
50. Hirota CL, McKay DM, M3 muscarinic receptor-deficient mice retain bethanechol-mediated intestinal ion transport and are more sensitive to colitis. Can J Physiol Pharmacol 84, 1153–1161 (2006). [PubMed: 17218980]
51. Takahashi T et al. , Non-neuronal acetylcholine as an endogenous regulator of proliferation and differentiation of Lgr5-positive stem cells in mice. FEBS J 281, 4672–4690 (2014). [PubMed: 25143155]
52. Labed SA et al. , Intestinal Epithelial Wnt Signaling Mediates Acetylcholine-Triggered Host Defense against Infection. Immunity 48, 963–978 e963 (2018). [PubMed: 29768179]
53. Sujino T et al. , Tissue adaptation of regulatory and intraepithelial CD4(+) T cells controls gut inflammation. Science 352, 1581–1586 (2016). [PubMed: 27256884]
54. Biton M et al. , T Helper Cell Cytokines Modulate Intestinal Stem Cell Renewal and Differentiation. Cell 175, 1307–1320 e1322 (2018). [PubMed: 30392957]
55. Dhawan S et al. , Acetylcholine-producing T cells in the intestine regulate antimicrobial peptide expression and microbial diversity. American journal of physiology. Gastrointestinal and liver physiology 311, G920–G933 (2016). [PubMed: 27514477]
56. Lutter L, Hoytema van Konijnenburg DP, Brand EC, Oldenburg B, van Wijk F, The elusive case of human intraepithelial T cells in gut homeostasis and inflammation. Nature reviews. Gastroenterology & hepatology 15, 637–649 (2018). [PubMed: 29973676]
57. Pickett JA, Edwardson JM, Compound exocytosis: mechanisms and functional significance. Traffic 7, 109–116 (2006). [PubMed: 16420520]
58. Freeman JA, Goblet cell fine structure. Anat Rec 154, 121–147 (1966). [PubMed: 4224216]

59. Freeman JA, Fine structure of the goblet cell mucous secretory process. Anat Rec 144, 341–357 (1962). [PubMed: 13959455]
60. Bauerfeind R, Huttner WB, Biogenesis of constitutive secretory vesicles, secretory granules and synaptic vesicles. Curr Opin Cell Biol 5, 628–635 (1993). [PubMed: 8257604]
61. Farquhar MG, Palade GE, The Golgi apparatus (complex)-(1954–1981)-from artifact to center stage. J Cell Biol 91, 77s–103s (1981). [PubMed: 7033246]
62. Trillo-Muyo S et al. , Granule-stored MUC5B mucins are packed by the non-covalent formation of N-terminal head-to-head tetramers. The Journal of biological chemistry 293, 5746–5754 (2018). [PubMed: 29440393]
63. Javitt G et al. , Assembly Mechanism of Mucin and von Willebrand Factor Polymers. Cell 183, 717–729 e716 (2020). [PubMed: 33031746]
64. Quinton PM, Cystic fibrosis: impaired bicarbonate secretion and mucoviscidosis. Lancet 372, 415–417 (2008). [PubMed: 18675692]
65. Seok J et al. , Genomic responses in mouse models poorly mimic human inflammatory diseases. Proceedings of the National Academy of Sciences of the United States of America 110, 3507–3512 (2013). [PubMed: 23401516]
66. Rivera J, Tessarollo L, Genetic background and the dilemma of translating mouse studies to humans. Immunity 28, 1–4 (2008). [PubMed: 18199409]
67. Wehkamp J et al. , Reduced Paneth cell alpha-defensins in ileal Crohn's disease. Proceedings of the National Academy of Sciences of the United States of America 102, 18129–18134 (2005). [PubMed: 16330776]
68. Liu TC et al. , Paneth cell defects in Crohn's disease patients promote dysbiosis. JCI Insight 1, e86907 (2016). [PubMed: 27699268]
69. van Doorninck JH et al. , A mouse model for the cystic fibrosis delta F508 mutation. The EMBO journal 14, 4403–4411 (1995). [PubMed: 7556083]
70. Shaner NC et al. , Improved monomeric red, orange and yellow fluorescent proteins derived from Discosoma sp. red fluorescent protein. Nature biotechnology 22, 1567–1572 (2004).
71. Schmieder R, Edwards R, Quality control and preprocessing of metagenomic datasets. Bioinformatics 27, 863–864 (2011). [PubMed: 21278185]
72. Dobin A et al. , STAR: ultrafast universal RNA-seq aligner. Bioinformatics 29, 15–21 (2013). [PubMed: 23104886]
73. Anders S, Pyl PT, Huber W, HTSeq--a Python framework to work with high-throughput sequencing data. Bioinformatics 31, 166–169 (2015). [PubMed: 25260700]
74. Love MI, Huber W, Anders S, Moderated estimation of fold change and dispersion for RNA-seq data with DESeq2. Genome biology 15, 550 (2014). [PubMed: 25516281]
75. Butler A, Hoffman P, Smibert P, Papalexi E, Satija R, Integrating single-cell transcriptomic data across different conditions, technologies, and species. Nature biotechnology 36, 411–420 (2018).
76. Stuart T et al. , Comprehensive Integration of Single-Cell Data. Cell 177, 1888–1902 e1821 (2019). [PubMed: 31178118]
77. Tinevez JY et al. , TrackMate: An open and extensible platform for single-particle tracking. Methods 115, 80–90 (2017). [PubMed: 27713081]

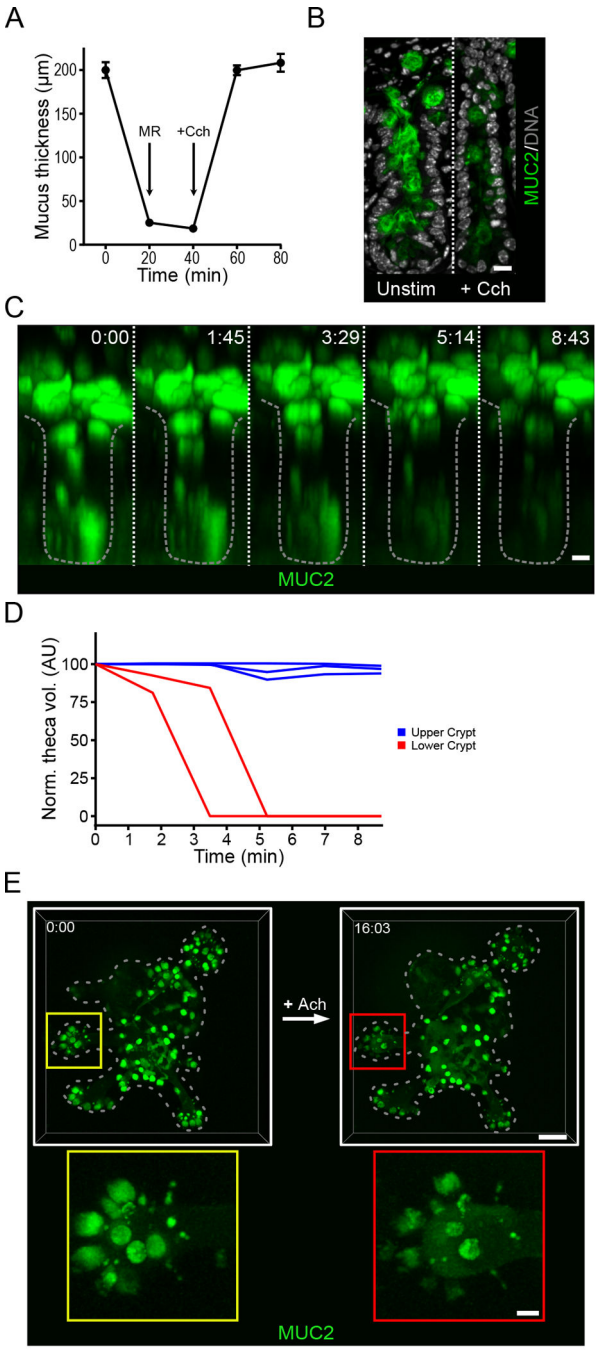

Fig. 1. Cholinergic stimulation of the small intestine induces a crypt-specific secretory response.

(**A**) Mucus thickness in mouse ileum immediately after explanation (time 0), after mucus removal (MR) at 20 min, and at the indicated time points after the tissue was stimulated by basal perfusion with carbachol (Cch) at 40 minutes. Data presented as mean ± SD (n = 5 independent experiments). (**B**) Immunofluorescence staining for Muc2 in goblet cells in the crypts of unstimulated (Unstim) and Cch-stimulated ileal explant tissue. Scale bar, 10 µm. Image is representative of 3 independent experiments. (**C**) Multi-photon live tissue imaging of small intestinal crypts from RedMUC2^{98tr} mice) after the tissue was stimulated with Cch

at time 0. Scale bar, 10 μm. Images are representative of n = 3 independent experiments. (**D**) Quantification of theca volume of individual mCherry^{+} cells from the crypt in panel C. (**E**) Live confocal imaging of ileal organoids generated from RedMUC2^{98tr} mice and stimulated with acetylcholine (Ach). Scale bar, 50 μm (main images) and 10 μm (insets). Images are representative of n = 3 independent experiments.

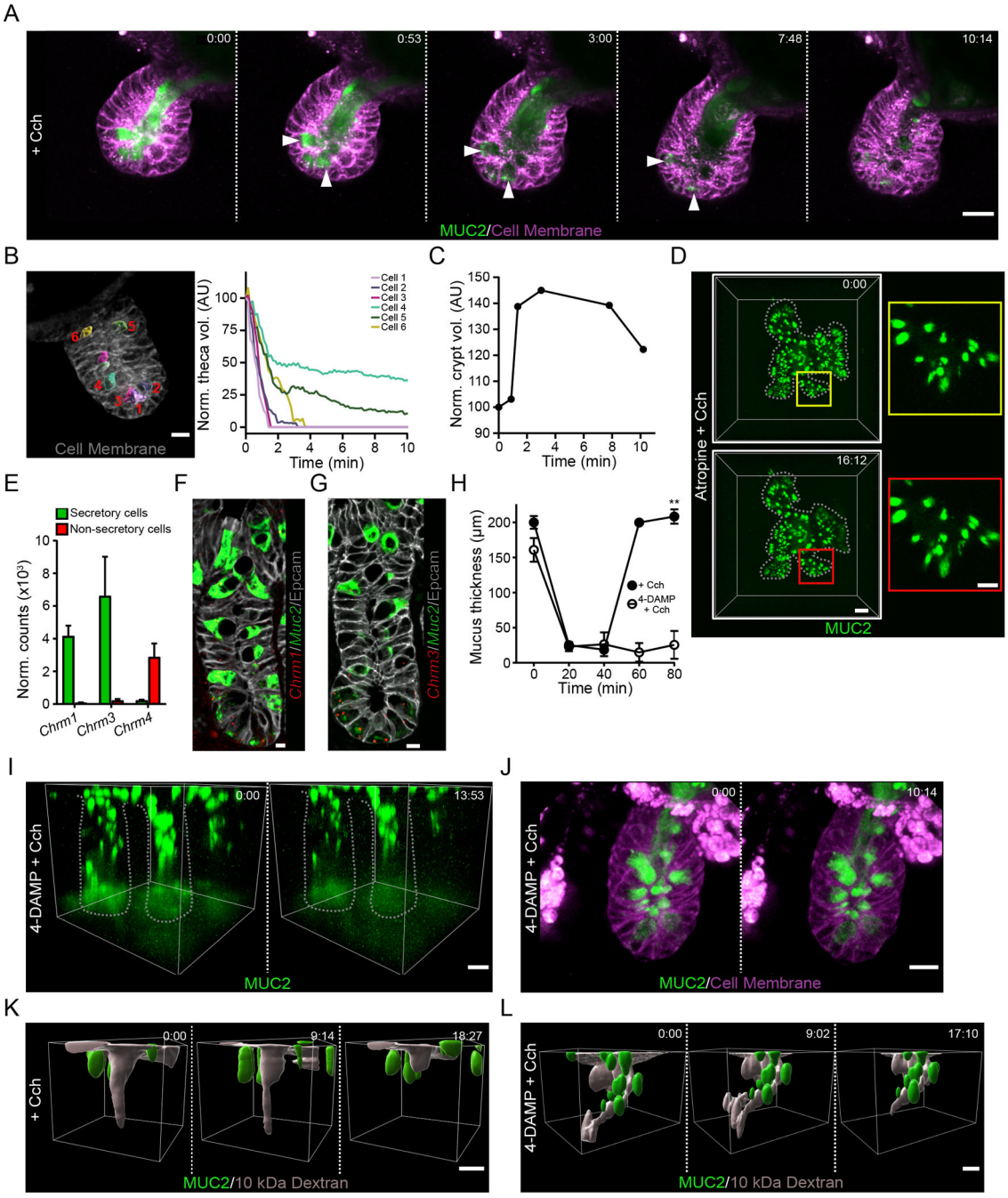

Fig. 2. The cholinergic secretory response flushes the crypt lumen.

(**A**) Live cell imaging of an organoid generated from RedMUC2^{98tr} mice and stimulated with carbachol (Cch) at time 0. White arrowheads indicate Cch-responsive mCherry-MUC2^{+} goblet cells. Scale bar, 20 µm. Images are representative of n = 5 independent experiments. (**B**) Analysis of goblet cell theca volume after stimulation of an ileal organoid with Cch. The image shows a representative crypt at time 0 with theca highlighted in individual numbered goblet cells using iso-surface analysis. Scale bar, 10 µm. The graph displays tracking of theca volumes of the individual cells after stimulation and normalized to the

volume at time 0. Image is representative of 3 independent experiments. (**C**) Quantification of crypt volume by iso-surface analysis in an organoid stimulated with Cch at time 0. Data are representative of 3 independent experiments. (**D**) Live confocal imaging of an ileal organoid stimulated with Cch at time 0 in the presence of the muscarinic receptor antagonist atropine. Scale bar, 50 μm (main images) and 20 μm (insets). Images are representative of n = 3 independent experiments. (**E**) RNA-seq analysis of expression of transcripts encoding muscarinic acetylcholine receptors in the small intestine from published RNA-seq data (13). (**F and G**) RNAscope analysis of *Muc2* and *Chrm1* (F) or *Chrm3* (G) in the mouse ileal crypt. Scale bar, 5 μm. Images are representative of 3 independent experiments. (**H**) Mucus thickness in small intestine explants stimulated with Cch in the absence or presence of the M_3-selective antagonist 4-DAMP. Mucus was removed from the tissue at 20 min, and Cch stimulation was performed at 40 min. Data presented as mean ± SD. (n = 5 independent experiments; ** $P < 0.01$, Mann-Whitney test). (**I**) Live tissue multi-photon imaging of MUC2 in crypts of ileal explants from RedMUC2^{98tr} mice that were pretreated with 4-DAMP before stimulation with Cch. The low fluorescence at the base of the crypt is due to photobleaching. Scale bar, 20 μm. Data are representative of n = 3 independent experiments. (**J**) Live cell imaging of RedMUC2^{98tr} organoid crypt following treatment with 4-DAMP and stimulation with Cch. Scale bar ,20 μm Images are representative of n = 3 independent experiments. (**K and L**) Live tissue imaging of Cch-induced ileal crypt flushing in tissue explanted from RedMUC2^{98tr} mice, labelled with soluble fluorescent dextran, and stimulated with Cch without (K) or with (L) 4-DAMP pretreatment. Scale bar, 20 μm. Images are representative of n = 3 independent experiments.

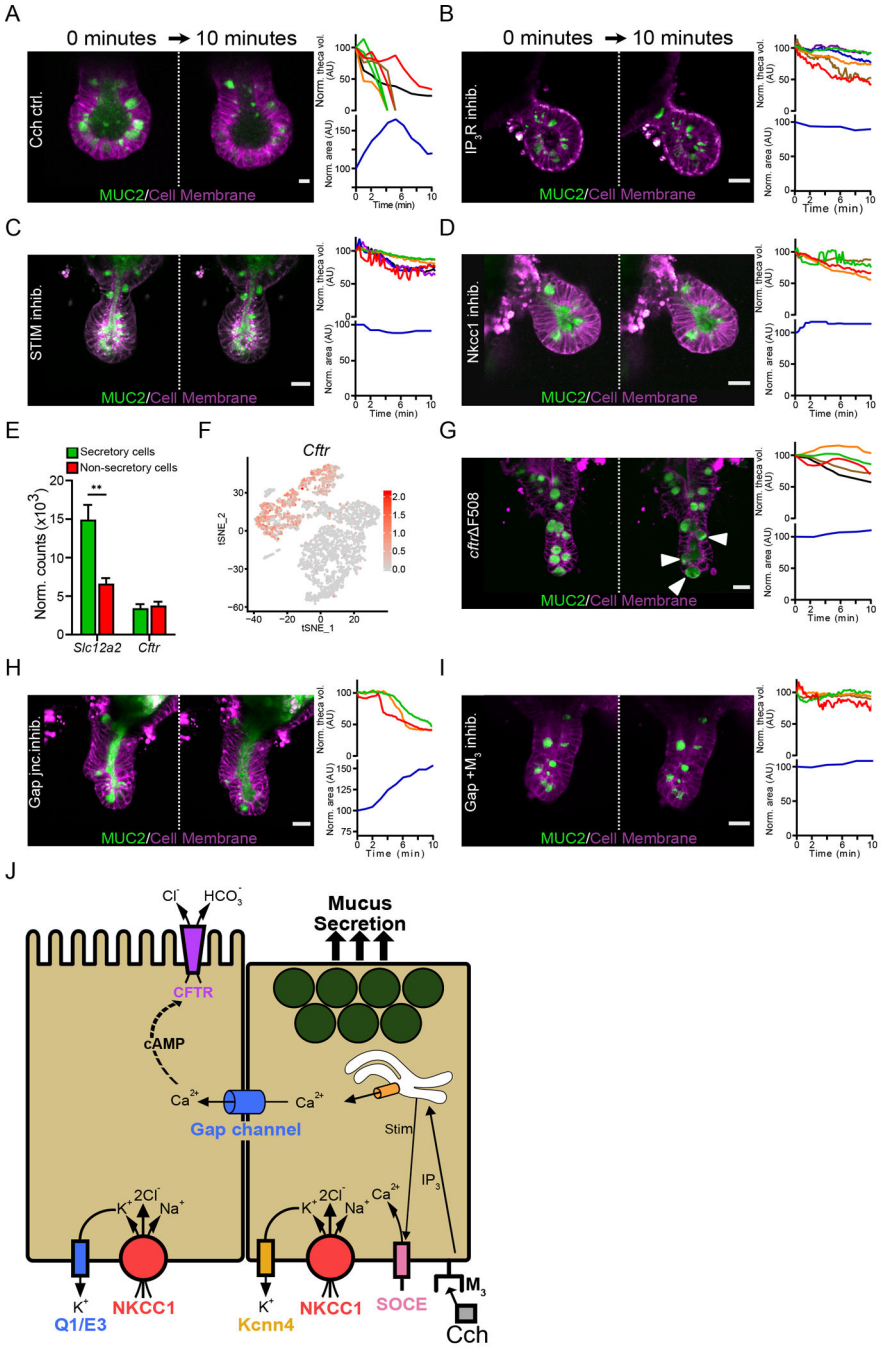

Fig. 3. Cholinergic stimulation induces a coordinated mucus and fluid secretory response.

(A) Live cell imaging of RedMUC298tr organoid crypts following stimulation with Cch. The graphs show quantification of theca volume for individual goblet cells and the crypt lumen area measurements with respect to time. Scale bar, 10 μm. (B to D) Live cell imaging and quantification of goblet cell theca volume and crypt volume in RedMUC298tr organoid crypts stimulated with Cch after pretreatment with the IP3R inhibitor Xestospongin C (B), the STIM inhibitor SKF 96365 (C), or the Nkcc1 inhibitor Bumetanide (D). Scale bars, 20 μm. Images in (A) to (D) are representative of n = 3 independent experiments.

(E) Quantification of Slc12a2 and Cftr expression in the small intestinal epithelium from published RNA-seq data (13) (** $P < 0.01$, Welch's test). (F) Single-cell mRNA cluster analysis of Cftr expression in small intestinal goblet cells from published single-cell RNA-seq data (13). (G to I) Live cell imaging of RedMUC298TR/CftrΔF508 organoids stimulated with Cch (G) or stimulated with Cch after pretreatment with the gap junction inhibitor carbenoxolone (H) or carbenoxolone plus the M3 receptor antagonist 4-DAMP (I). Scale bars, 20 μm. Images in (G) to (I) are representative of $n = 3$ independent experiments. (J) Graphical summary of the role of Ca2+ signaling, gap channel cell-to-cell communication, and ion transport on mucus secretion.

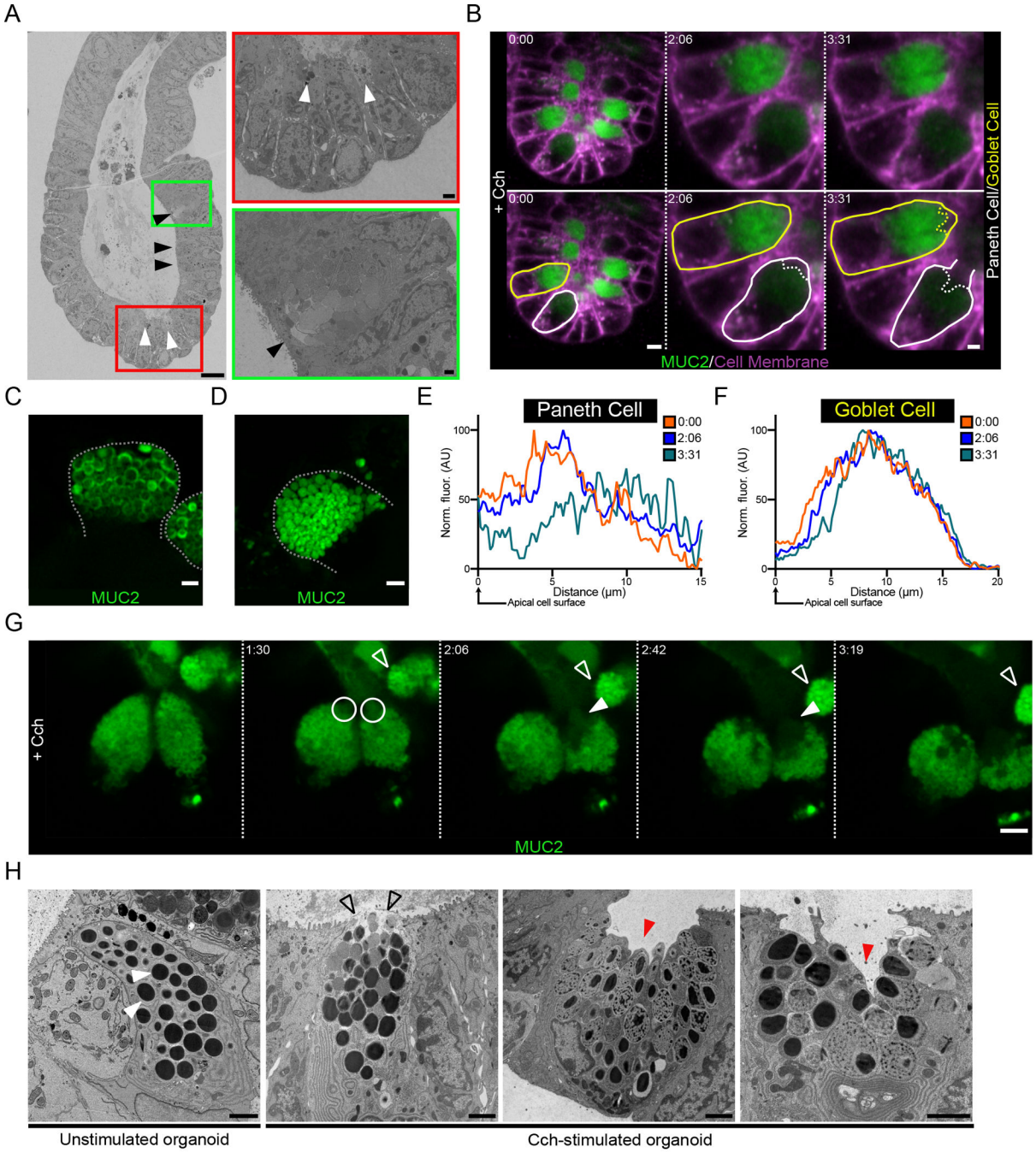

Fig. 4. The crypt secretory response to cholinergic stimulation occurs in an ordered manner.

(**A**) Scanning electron micrograph of a crypt from a Cch-stimulated organoid. Paneth cells are indicated by white arrowheads, and goblet cells are indicated by black arrowheads. Scale bars, 10 μm (main image), 1 μm (red inset), 2 μm (green inset). Images are representative of 3 independent experiments. (**B**) Live cell imaging of a RedMUC2^{98TR} organoid crypt base following cholinergic stimulation. Images are shown in duplicate with no labelling and with goblet (yellow) and Paneth (white) cells outlined. Scale bars, 10 μm (Time 0:00) and 5 μm (Time 2:06 & 3:31). Images are representative of 3 independent experiments. (**C**

and D) High-resolution image of Paneth cell (C) and goblet cell (D) secretory granules in a RedMUC2^{98TR} organoid. Scale bar, 2 μm. Images are representative of 3 independent experiments. (**E and F**) Line profile quantification of theca fluorescence of the Paneth cell (E) and goblet cell (F) outlined in (B) following Cch stimulation. Data are representative of 3 independent experiments. (**G**) High-resolution live cell imaging of organoid Paneth cell following Cch stimulation. White circles and closed arrowheads highlight secretion of material from Paneth cells. Open arrowhead highlights adjacent goblet cell. Scale bar 5 μm. Images are representative of n = 3 independent experiments. (**H**) Electron micrographs of Paneth cells from unstimulated and Cch-stimulated organoids. White arrowheads indicate resting Paneth cell granules. Open arrowheads highlight release of apical granules. Red arrowheads indicate retention of basal secretory granules. Scale bars, 2 μm. Images are representative of 3 independent experiments.

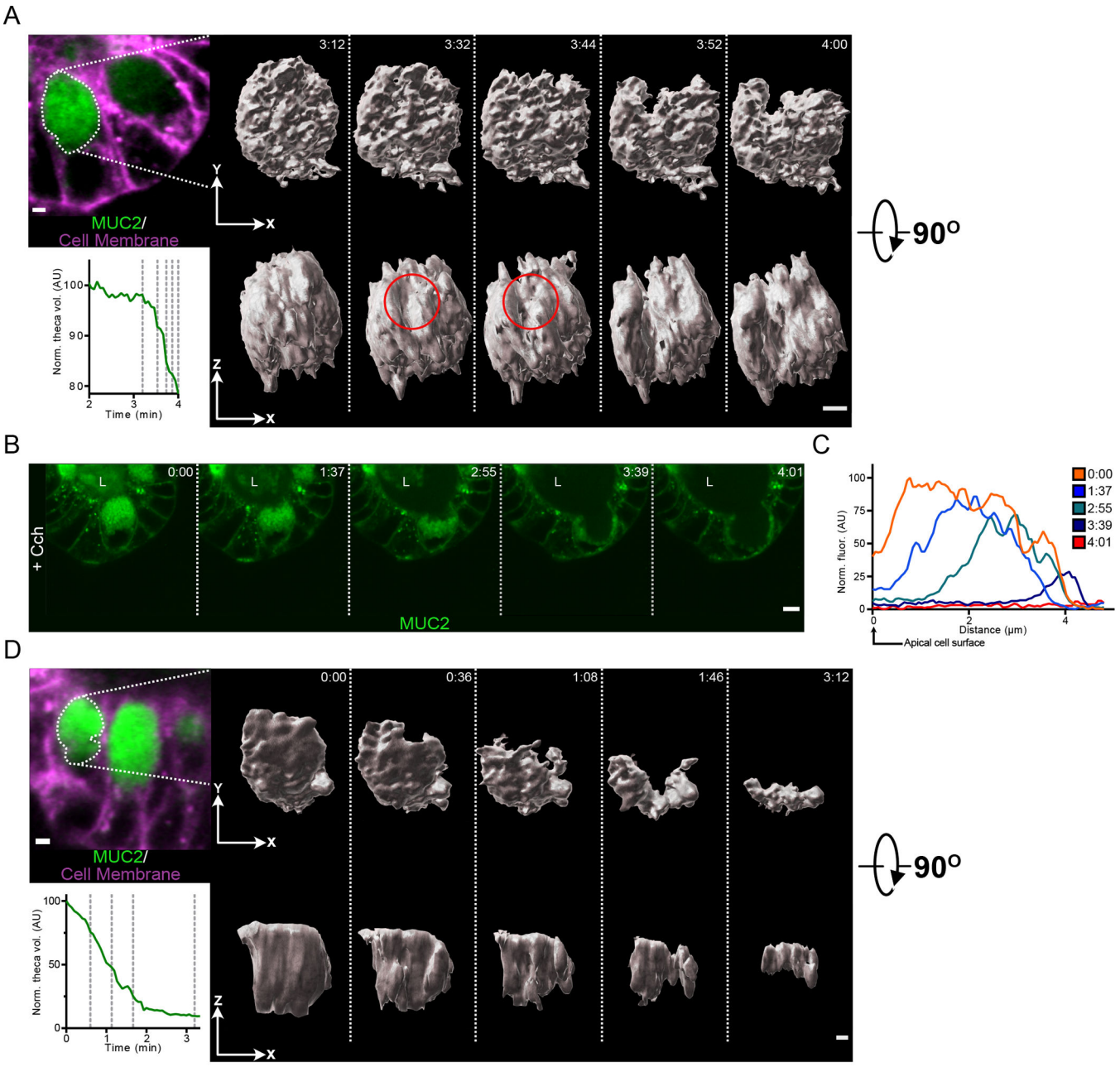

Fig. 5. Granules in the goblet cell theca are secreted in an ordered manner in response to Cch stimulation.

(A) Micrograph shows a goblet cell of a RedMUC298TR organoid prior to Cch treatment with the theca outlined. Graph displays the normalized theca volume of the highlighted goblet cell during the initiation of secretion following Cch stimulation. The vertical dashed lines in the graph indicate the time points for which iso-surface reconstructions of the goblet cell theca are shown. The red circle indicates the region within the theca where the secretory response initiates. Scale bar, 2 μm. Data are representative of 3 independent experiments. (B) High-resolution live cell imaging of a RedMUC298TR organoid crypt goblet cell after Cch stimulation. L, crypt lumen. Images are representative of n = 3 independent

experiments. Scale bar, 5 μm. (C) Line profile quantification of theca fluorescence of goblet cell shown in panel (B) following Cch stimulation. (D) Micrograph shows a goblet cell of a RedMUC298TR organoid prior to Cch treatment with the theca outlined. Graph displays the normalized theca volume of the highlighted goblet cell throughout the secretory event following cholinergic stimulation. The vertical dashed lines in the graph indicate the time points for which iso-surface reconstructions of the goblet cell theca are shown. Scale bar, 2 μm. Data are representative of 3 independent experiments.

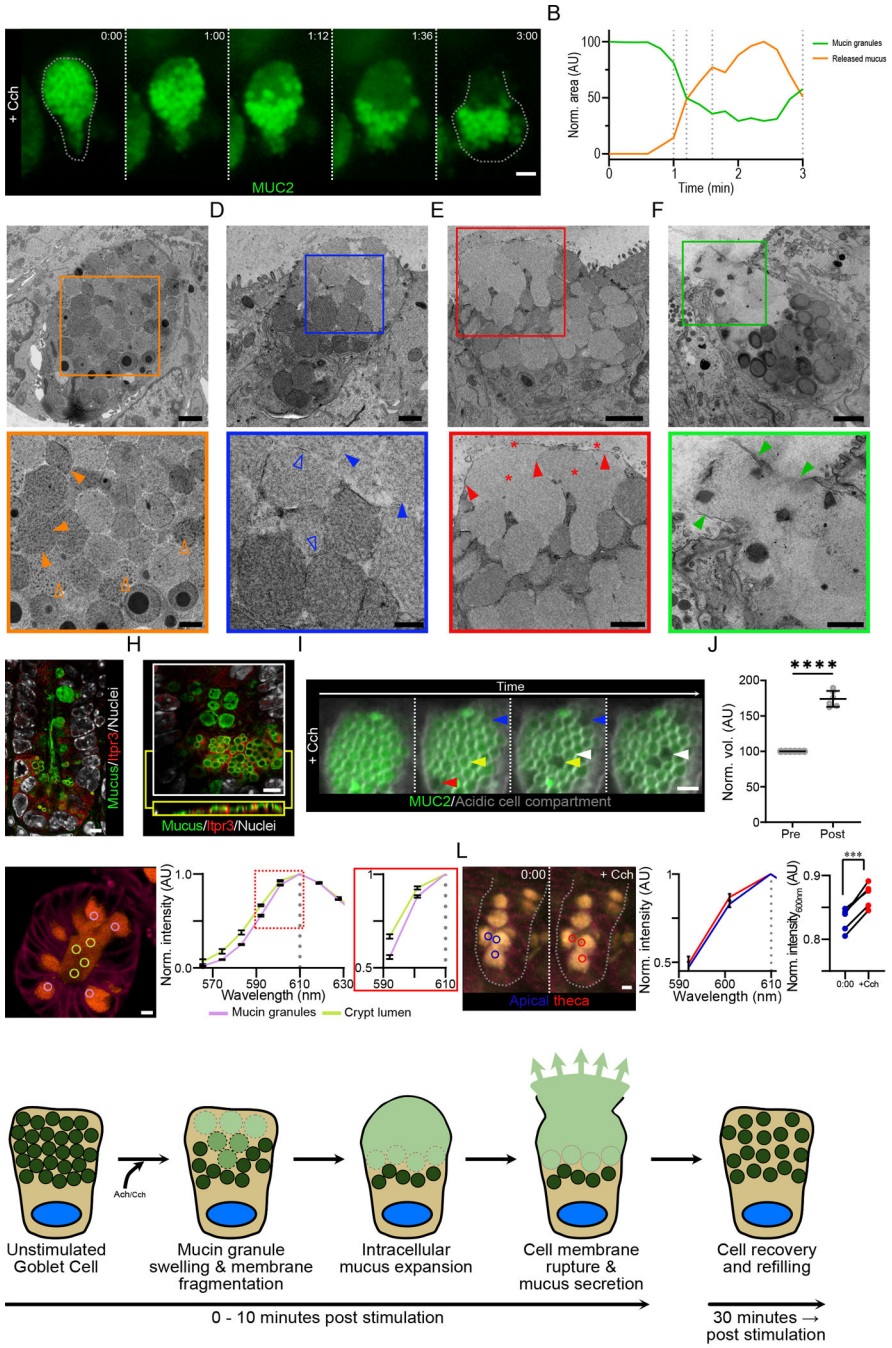

Fig. 6. The goblet cell secretory response to Cch involves the intracellular release of mucin granule contents prior to the secretion of mucus.

(**A**) High resolution live cell imaging of crypt goblet cell in a RedMUC2^{98TR} organoid in response to Cch stimulation. Dashed lines images indicate the cell border. Scale bar, 5 μm. Data are representative of n = 3 independent experiments. (**B**) Fluorescence quantification of mucin granules and intracellular mucus in the cell in (A). (**C**) Transmission electron micrograph of a goblet cell from an unstimulated small intestine organoid. Closed orange arrowheads highlight inter-granule membrane interactions, and open orange arrowheads

indicate condensed intra-granule mucus material. Scale bars, 2 μm (main image) and 1 μm (inset). (**D to F**) Transmission electron micrographs of Cch-stimulated organoid goblet cells. Closed blue arrowheads highlight the expansion of granule material, and open blue arrowheads indicate the presence of fragmented granule membranes (D). Closed red arrowheads highlight the presence of an intact apical cell membrane, and red stars indicate the presence of expanded mucus material (E). Closed green arrowheads highlight the disruption of the apical cell membrane during the exocytosis of mucus from the goblet cell (F). Scale bars, 1 μm (main image D) and 500 nm (inset D), 2 μm (main image E & F) and 1 μm (inset E & F). Images in (c) to (F) are representative of 3 independent experiments. (**G**) Confocal micrograph of small intestinal crypt stained for Itpr3, mucus, and nuclear counterstain. Mucus was stained with Alexa Fluor 647 conjugated wheat germ agglutin (WGA), which binds strongly to the highly glycosylated mucin glycoproteins. Scale bar, 5 μm. Image is representative of 3 independent experiments. (**H**) High resolution confocal micrograph of crypt bottom stained for Itpr3, mucus, and nuclear counterstain. An X/Y-axis cross section (white box) and an X/Z-axis cross section (yellow box) are shown. Scale bar, 5 μm. Image is representative of 3 independent experiments. (**I**) Live cell imaging of organoid goblet cell theca pretreated with LysoSensor Green dye (grey) before Cch stimulation. Arrowheads highlight mucin granules before and after expansion. Scale bar, 2 μm. Images are representative of n = 3 independent experiments. (**J**) Quantification of change in granule volume in cells treated as in (I) (**** $p < 0.001$, paired t-test of log transformed values, n = 3 independent experiments) (**K**) Spectral analysis of luminal mucus (yellow circles) and granule mucus (lilac circles) in a resting RedMUC2^{98tr} organoid. Image is representative of 3 independent experiments. (**L**) Spectral analysis of thecal mucus in a RedMUC2^{98tr} organoid following stimulation with Cch. Blue circles mark areas in apical theca before stimulation; red circles mark areas in apical theca approximately 1 minute post stimulation. Graphs show mCherry emission spectra (590– 610 nm) before and after Cch stimulation and emission intensity changes at 600 nm in individual goblet cells from one out of three representative experiments (*** $p = 0.0005$, paired t-test; n = 3). (**M**) Graphical summary of the steps involved in the crypt goblet cell response to cholinergic stimulation.